Spring 2017

Bio-inspired flow fields for pem fuel cells- decoupling pressure and distribution effects on performance and identifying design opportunities

Joshua David Heck

Department:

BIO-INSPIRED FLOW FIELDS FOR PEM FUEL CELLS– DECOUPLING PRESSURE AND DISTRIBUTION EFFECTS ON PERFORMANCE AND IDENTIFYING DESIGN OPPORTUNITIES

by

JOSHUA DAVID HECK

A THESIS

Presented to the Graduate Faculty of the

MISSOURI UNIVERSITY OF SCIENCE AND TECHNOLOGY

In Partial Fulfillment of the Requirements for the Degree

MASTER OF SCIENCE

in

MECHANICAL ENGINEERING

2017

Approved by

Umit O. Koylu, Co-Advisor
Ming C. Leu, Co-Advisor
Kelly O. Homan

PUBLICATION THESIS OPTION

This thesis consists of the following two articles which have been submitted for publication, or will be submitted for publication as follows:

Paper I: Pages 7-39 have been submitted to the International Journal of Hydrogen Energy.

Paper II: Pages 40-77 are intended for submission to the International Journal of Hydrogen Energy.

ABSTRACT

The performance of Polymer Electrolyte Membrane Fuel Cells (PEMFCs) is significantly impacted by flow distributor geometry. The effects of flow distributor geometry on PEMFCs was explored in two ways in this study. Firstly, the relative effects of pressure and distribution characteristics of different flow fields on fuel cell unit and system level performance were considered. A method of decoupling these effects was proposed and demonstrated by application to the traditional serpentine and parallel flow field designs. The performance of these two designs were modeled computationally and it was shown that, of the 17% better performance of the serpentine design, 12% was due to mass transport effects, while 5% was due to the effect of increased pressure loss. Secondly, the idea of Bio-Inspired design for creating new fuel cell flow field geometries was investigated to determine the window of opportunity in fuel cell applications for gaining maximum benefit from bio design. It was determined that the area of opportunity for bio design was when having a minimal pressure loss across the flow field was a dominate design constraint. A set of design principles for creating bio flow fields under this design constraint was developed. These principles were then demonstrated by creating an example bio flow field, and simulating its performance computationally, along with that of the traditional parallel design as a reference. The bio design was shown to have lower pressure losses which allowed it to produce 2-3 times better power output per pumping power input than the parallel design, while also maintaining better reactant distribution. Lastly, a new method of determining operating conditions when using low humidity supply gas was developed to help alleviate water management issues. This method, which has been termed Water Balanced operation, was tested on both the bio and parallel design, and was shown to improve performance in both cases.

ACKNOWLEDGMENTS

I would like to thank my co-advisors, Dr. Umit Koylu and Dr. Ming Leu, for providing me with the guidance and all of the resources that I required to succeed in completing my MS degree. I would also like to thank the Department of Mechanical and Aerospace Engineering and Dr. Ashok Midha for providing me with a Graduate Teaching Assistantship during the course of pursuing my MS degree, and the Chancellor's Fellowship for funding my course work.

I would also like to thank the Missouri S&T FORGE cluster admins on the S&T Research Support Services group, specifically Nicholas Eggleston and Buddy Scharfenberg, for going above and beyond to help sort out the issues of running my computations on the cluster. I could not have completed my work on time if not for their help.

The research for this thesis was supported by the Missouri University of Science and Technology's Innovation Initiative, and the Intelligent System Center at Missouri S&T, and I would like thank those sources for supporting my work.

Finally, thanks to my wife, Hope, for putting up with my crazy schedule, and helping me push through the times when I thought I had bitten off more than I could chew.

TABLE OF CONTENTS

Page

LIST OF ILLUSTRATIONS

LIST OF TABLES

SECTION

1. INTRODUCTION

1.1. PROTON EXCHANGE MEMBRANE FUEL CELLS

In the ongoing search for cleaner and more efficient power generation methods, fuel cells have emerged as a promising candidate. Fuel cells work on the principle of direct energy conversion, utilizing electrochemical reactions to produce electrical power from the chemical potential of a fuel in a single step. There are many types of fuel cells, but among them, Proton Exchange Membrane Fuel Cells (PEMFCs) are particularly promising due to their low operating temperature, fast startup, and quiet operation. A cross section view of a typical PEMFC is shown in Figure 1.1.

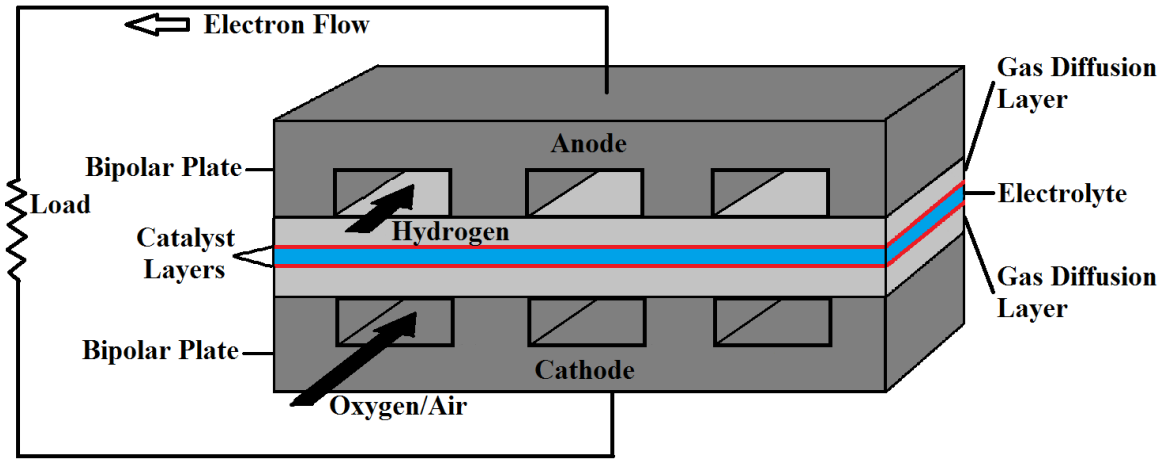

Figure 1.1. Cross Section of a PEMFC

The heart of the PEMFC is the Membrane Electrode Assembly (MEA), consisting of the electrolyte membrane with catalyst layer coating on either side, sandwiched between the Gas Diffusion Layers (GDLs), which are typically made of porous carbon paper or cloth. It is only at the catalyst layers that the electrochemical half reactions occur, as

$$Anode : H_2 \rightarrow 2H^+ + 2e^-, \tag{1.1}$$

$$Cathode : \frac{1}{2}O_2 + 2H^+ + 2e^- \rightarrow H_2O. \tag{1.2}$$

For this reason, the planar projection of the catalyst layers is called the "active area" of the fuel cell. Hydrogen is supplied to the anode and passes through the pores of the anode GDL to complete the anode half reaction at the catalyst layer. Protonic transport then occurs across the membrane, carrying H^+ ions from anode to cathode, while the solid material of the GDL transports the electrons away from the catalyst layer to pass through the external load circuit. Oxygen supplied at the cathode, often in the form of air, travels through the pores of the cathode GDL to the cathode catalyst layer. Here, the oxygen combines with the H^+ ions and e^- electrons to participate in the cathode half reaction producing water and some waste heat, which are the only bi-products of PEMFC operation.

The MEA is sandwiched between a pair of Bipolar Plates (BPP). These plates have a set of channels in their surfaces contacting the GDL that serve as the flow distributors for the fuel and oxidizer, while the ribs between channels serve to collect the current from the GDL. (For this reason, they are also called current collector plates.)

Fuel cells posses some of the most attractive features of fuel based power production and battery energy storage for both stationary and portable applications. By skipping the multiple conversions of energy typically seen in conventional fuel based power generation (chemical potential, to heat, to mechanical work and finally to electrical power) fuel cells can operate at much higher efficiency than traditional methods. They operate as silently as batteries since they have no moving parts, and in a similar temperature range, with

temperatures staying below the boiling point of water. However, unlike batteries, since they are still fuel based power production devices, not merely energy storage devices, they can run continuously, given sufficient supply of fuel and oxidizer, without need for down time to re-charge. This is especially beneficial in portable electrical applications where range is often limited by battery capacity. Finally, as has been mentioned, the only bi-products of fuel cells are heat and water, so no harmful emissions are produced in their operation.

1.2. IMPORTANCE OF FLOW DISTRIBUTORS

Despite all of these positive attributes, fuel cells have not yet achieved significant market penetration. This is due in part to the fact that PEMFCs have yet to achieve the level of durability and reliability required to replace conventional methods of power production which have the advantage of decades of development. One of the critical contributors to fuel cell degradation is non-uniform distribution of reactants over the active area, causing non-uniform reactions. This leads to build up of product water in some locations (flooding), dry spots in other locations, and hot spots in the fuel cell, all of which cause mechanical degradation of the membrane. The key component in achieving good reactant distribution in the fuel cell are the flow distributor channels in the BPPs.

Furthermore, maldistribution not only affects durability but also operating performance of the fuel cell. The flow distributor channels are responsible for both supplying fresh reactants to, and removing product water from the reaction zones. Any region which is under supplied with fresh reactants or clogged with product water accumulation will be poorly utilized. These areas, often referred to as “dead spots”, effectively reduce the active area of the fuel cell, and performance suffers accordingly. Therefore, the geometry of the flow channels is very important to both immediate and long-term fuel cell performance, and as such flow field design is an active field of research.

1.3. PRESSURE EFFECTS ON FUEL CELL PERFORMANCE

Not only does the geometry of the flow channels play a leading role in the distribution of reactants but also determines the total pressure loss which will occur across the flow field, and the local pressure distribution over the active area. The total pressure loss corresponds directly to power consumption of the auxiliary system required to operate a fuel cell. The auxiliary system power requirement can be considered a parasitic loss to system performance so it is desirable to reduce auxiliary power as much as possible. However, having a high pressure drop across the fuel cell serves to raise the average operating pressure of the cell, which increases cell performance through increased reactant molar concentration.

Since these factors influence fuel cell system performance in opposite ways, they must both be taken into consideration to determine the overall effect. However, in past works on flow field performance, there has not been a consistent method for comparison of different flow field geometries. When comparing the performance of various flow fields to one another, all performance variation is commonly attributed to reactant distribution only, and one or both of these pressure effects is often neglected. In this thesis, the relative effects of reactant distribution and pressure characteristics of flow field geometry on fuel cell system performance were explored in detail, and a methodology was proposed for comparing the performance of different flow field geometries which decouples all pressure effects from those of reactant distribution.

1.4. BIO-INSPIRED DESIGN FOR FLOW FIELDS

As previously mentioned, flow field design is an active field of research for improving fuel cell performance, durability, and reliability. The idea of Bio-Inspired design is a promising strategy which has emerged in recent years. The idea behind bio design is that

there exist similarities of operation in biological flow systems and fuel cell flow distributors. Biological flow systems perform very effectively, and so aspects of these designs already found in nature can be mimicked to improve fuel cell flow field performance.

A number of works have been published making use of bio design strategy. These past studies mostly focus on the physical geometry of biological flow structures, and how aspects of their geometry can be incorporated into fuel cell flow fields. This is often done without delving into the performance requirements of biological flow structures which determine their geometry in the first place. If mimicking the geometry of biological flow systems is going to enhance flow field performance, the performance requirements of the fuel cell flow field must be the same as those of biological flow structures. This means that the application of bio design will only be beneficial to fuel cell performance if the operating requirements match those of biological systems. In the wide range of applications for which fuel cells are suited, this is not always the case. In this work, the dominating performance requirements of biological flow systems were investigated. Those performance goals were used to determine the window of opportunity in fuel cell flow field design that fits the strengths of bio deisgn. Furthermore, a set of design principles for creating flow fields was then developed to take maximum advantage of the strengths of biological flow systems in the operating widow identified. The performance of the bio deisign was compared to that of the traditional parallel design as a reference.

Finally, the performance of the bio and traditional parallel designs were tested under low humidity cathode supply gas operation, in which mode water management issues of both membrane dehydration and flooding could be of concern. In order to alleviate the water management issues, a new method of determining the operating conditions was proposed which has been termed Water Balanced (WB) operation, and was tested on both bio and traditional parallel designs.

1.5. SUMMARY OF THE PRESENT WORK

This thesis is composed of two journal papers which have been, or will be, submitted for publication. The first paper focuses on the relative effects of pressure and flow distribution on the performance of fuel cell systems. The effects of pressure on both the fuel cell unit and auxiliary system are modeled and discussed, and a method for decoupling pressure and distribution effects on fuel cell system performance is proposed and demonstrated. The second paper focuses on the applicability of bio design to fuel cell flow fields. The main performance requirements of biological flow structures, which determine their geometry, and the key geometric characteristics, which allow biological flow structures to meet these performance requirements, are identified. This information is used to explore the widow of opportunity for bio design to fuel cell flow fields by matching performance requirements, and to develop a set of design principles for creating bio flow fields by using similar geometric characteristics. The design principles are then demonstrated by creating and testing an example bio design. In order to test the application of proposed methods and design principles in these two works, analytical and computational modeling were employed to predict the performance of fuel cells using various flow fields.

PAPER

I. DECOUPLING PRESSURE AND DISTRIBUTION EFFECTS ON THE PERFORMANCE OF POLYMER ELECTROLYTE FUEL CELLS

Joshua D. Heck, Warren S. Vaz, Umit O. Koylu, Ming C. Leu

Department of Mechanical & Aerospace Engineering

Missouri University of Science and Technology

Rolla, Missouri 65409–0050

Tel: 573–466–3428, Fax: 573–341–4607

Email: jdh26c@mst.edu

ABSTRACT

The performance of Polymer Electrolyte Membrane Fuel Cells (PEMFCs) is highly dependent on the flow distribution and pressure of reactant gases. Existing studies on comparison of flow field designs have not fully taken into account the degree to which the pressure loss across different flow field designs affects the performance of a fuel cell system, rather attributing performance of flow fields to mass transport characteristics only. In this work, the relative importance of differing supply pressure requirements of flow field designs in PEMFCs is considered. A thermodynamic First-Law analysis of the auxiliary system is developed in order to demonstrate how the pressure drop affects all auxiliary system components and fuel cell unit performance. A method of comparison is then proposed to eliminate the effects of pressure in the comparison of fuel cells with different flow field designs. This method is applied to the single serpentine and parallel designs by Computational Fluid Dynamics (CFD) simulation. It is shown that, of the serpentine design's 17.1 % better performance, mass transport effects provide 12.2 % improvement, and pressure effects ac-

count for the remaining 4.9 %. Since increased pressure loss across the flow field has both positive and negative effects on system performance, decoupling pressure and distribution effects is critical in comparing different flow fields. Finally, a metric is proposed by which the relative effect of pressure between different designs may be estimated for past results not using the recommended method, and is demonstrated by application to results found in existing literature.

Keywords: polymer electrolyte membrane (PEM); fuel cell; flow distributor design; computational fluid dynamics (CFD); First Law Analysis; system performance comparison

Highlights

- Discussed impacts of pressure drop on auxiliary system and inlet mixture properties
- Showed that pressure effects can have significant impact on fuel cell performance
- Proposed a method for decoupling pressure/distribution effects on fuel cell performance
- Demonstrated the method of decoupling in comparison of serpentine and parallel designs

Table 1. Nomenclature

Symbol	Meaning	Units
A_{act}	Active Area	cm^2
$[C_i]$	Concentration of Reacting Species at Catalyst	$mol\ m^{-3}$
$[C_{i,ref}]$	Reference Concentration of Reacting Species	$mol\ m^{-3}$
c_p	Constant Pressure Specific Heat	$J\ kg^{-1}K^{-1}$
F	Faraday's Constant	$C\ mol^{-1}$
h_{fg}	Enthalpy of Vaporization of Water	$kJ\ kg^{-1}$
I_{H_2}	Total Current Produced Based on Hydrogen Consumption	$Amperes(A)$
I_{O_2}	Total Current Produced Based on Oxygen Consumption	$Amperes(A)$
J	Volumetric Current Generation	$A\ m^{-3}$
j	Current Density per unit Area	$A\ cm^{-2}$
j_{ref}	Reference Exchange Current Density	$A\ m^{-2}$
k	Ratio of Specific Heats	
M_i	Average Molecular Weight of Dry Gas Mixture i	$kg\ mol^{-1}$
M_j	Molecular Weight of Species j	$kg\ mol^{-1}$
$\dot{m}_i$	Mass Flow Rate of Dry Gas Mixture i	$kg\ s^{-1}$
$\dot{m}_{w,i}$	Mass Flow Rate of Water to Humidify Dry Gas Mixture i	$kg\ s^{-1}$
$\Delta\dot{m}_{H_2}$	Mass Consumption Rate of Hydrogen	$kg\ s^{-1}$
$\Delta\dot{m}_{O_2}$	Mass Consumption Rate of Oxygen	$kg\ s^{-1}$
n_j	Number of Electrons Released per Reaction per Species j	
$\hat{P}$	Non-Dimensional Inlet Pressure	
P_0	Local Dead State Pressure	Pa
P_1	Pressure at Compressor Outlet Prior to Humidification	Pa
P_{in}	Pressure at Fuel Cell Inlet	Pa
P_i	Partial Pressure of Species i	Pa

Continuation of Table 1		
Symbol	**Meaning**	**Units**
$P_{v,in}$	Saturation Pressure of Water at the inlet Temperature	Pa
$\dot{Q}_i$	Power Required to Heat Dry Gas Mixture i	W
$\dot{Q}_{w,i}$	Power Required Evaporate Water to Humidify Dry Gas i	W
$\dot{Q}_{waste}$	Waste Heat Rejected from Fuel Cell	W
R	Universal Gas Constant	$J\,mol^{-1}K^{-1}$
T	Local Temperature	K
T_0	Dead State Temperature	K
T_1	Temperature at Compressor Outlet Prior to Humidification	Pa
T_{in}	Temperature at Fuel Cell Inlet	K
$\dot{W}_{aux,i}$	Total Auxiliary System Power Requirement	W
$\dot{W}_{c,i}$	Compressor Power to Pump Dry Gas i	W
$\dot{W}_{fc}$	Power Output of a Fuel Cell Unit	W
X_{H_2O}	Mole Fraction of Water Vapor	
Y_j	Mass Fraction of Species j	
Greek Symbols		
α	Transfer Coefficient	
γ	Concentration Exponent	
ζ	Catalyst Layer Surface to Volume Ratio	m^{-1}
η	Activation Overvoltage	$volts$
η_c	Compressor Efficiency	
ϕ_0	Relative Humidity of Dead State Air	
ϕ_1	Relative Humidity at Compressor Outlet Prior to Humidification	
ϕ_{in}	Relative Humidity at Fuel Cell Inlet	

Continuation of Table 1		
Symbol	**Meaning**	**Units**
ξ	Stoichiometry (Ratio of Reactant Supply to Amount Consumed)	
End of Table		

1. INTRODUCTION

In recent years, Proton Exchange Membrane Fuel Cells (PEMFCs) have emerged as a promising candidate in a widespread search to develop energy devices that are sustainable and have cleaner operation than traditional means of power generation, which rely heavily on the combustion of fossil fuels [1]. The only local product of PEMFC operation is water, and if clean methods are used to produce hydrogen, PEMFCs can have net-zero-emission power production [2]. Additionally, since PEMFCs are a direct energy conversion device, higher operating efficiencies can be realized than those attainable by conventional energy conversion methods that rely on intermediate heat steps [3].

Before fuel cells are widely accepted, further improvements in performance and durability need to be achieved. When operating a fuel cell, the inlet conditions may be set as desired, but the spatial variation of parameters which affect performance and durability are controlled by the mass and heat transport properties of the flow field and the porous Gas Diffusion Layer (GDL). For this reason, one of the key research areas in fuel cell development is the design of flow distributors in the bipolar plates. Effective distribution of reactants and product removal have a large impact on the performance and durability of PEMFCs [4–6]. Wang et al. [7, 8] noted that the thermal and water management issues, which also affect durability in PEMFCs, were mainly due to maldistribution of flow both at the stack and cell level and developed an analytical model, which may be applied to several common flow field arrangements for even distribution performance.

Numerous works have been presented that attempt either to characterize performance response to different flow distributor designs or to propose some new geometry for improving flow distribution. Some of the most well-studied conventional designs are the Parallel, Serpentine, and Interdigitated flow distributors. Depending on the configuration of the flow channels, both convective and diffusive flow can take place in the GDL. Mass transport across the GDL in the Parallel design is dominated by diffusion. The Interdigitated flow distributor proposed by Nguyen [9] does not have a direct connection between the inlet and outlet, and thus transport across the GDL is predominately convective, that is, the bulk flow is driven through the GDL due to a pressure gradient between adjacent inlet and outlet channels. Similar to the Parallel design, the channels of the Serpentine design are continuous from inlet to outlet, however, both local convective and diffusive transport take place in this design since appreciable pressure differences in adjacent channels develop due to the long flow path [10]. Chiu et al. [11] performed a comparative study on these three designs using computational methods in which they focused on the three designs' abilities to remove product water.

While the geometries of these three traditional designs are similar in form, many researchers have proposed alternative new geometries for flow distributors. Vazifeshenas et al. [12] proposed a compound flow field that utilizes the Serpentine configuration over part of the flow field and Parallel over the rest. Juarez-Robles et al. [13] proposed a flow distributor consisting of a number of concentric spiral channels. Guo et al. [14] performed a network based optimization of the channel sizes in the traditional pin type design, and in another work [15] proposed three variations on a bio-inspired design based on leaf vein patterns. Further work on characterizing the water transport characteristics of these bio-inspired designs was carried out by Saripella et al. [16]. The geometries of all of these designs are radically different from the traditional ones. Many additional studies have been published which attempt to characterize or improve some aspects of flow distributors [17–29].

With such widely varying geometry among previous works, there has not been a consistent method for the comparison of the performance of fuel cells utilizing different flow distributors. The most commonly used approach has been to set the same reactant gas inlet temperatures, mixture compositions, and the same back pressures at the anode and cathode outlet ports for the designs being considered. The polarization curves and peak power density for those conditions are obtained and compared. However, the pressure drop across a cell, which is controlled by the flow field geometry, affects the performance of a fuel cell system in several ways and these effects can make this common method of performance comparison insufficient.

In order for a fuel cell system to operate at a set of desired inlet conditions, an auxiliary system is required in order to pump, heat, and humidify the supply gases. The flow field geometry not only plays a major role in the variation of local conditions over the active area of a fuel cell but also determines the total pressure loss across the fuel cell. The energy lost in this pressure drop must be supplied by a compressor. Furthermore, the inlet pressure, which for some designs can be significantly different than the outlet pressure, impacts inlet mixture composition and properties, such as the required mass fraction of water to obtain a desired relative humidity. Any change in inlet mixture composition will in turn affect auxiliary power requirements, which may be considered a parasitic loss to the fuel cell system. Accordingly, ranking performance based on net fuel cell system power may produce results that are different from those seen when considering only gross fuel cell power [28]. Some studies have ignored these losses entirely [18, 30], while others have considered them to varying degrees, ranging from merely mentioning that the different designs induce different pressure losses [17] to calculating the net system power accounting for pumping losses [28]. However, the effects of pressure on all auxiliary system processes, not only pumping power but also heating and humidification, have not been considered in the literature.

In addition to its effect on auxiliary system power, another important consideration is the direct effect of inlet pressure on the fuel cell performance. The kinetic losses in a fuel cell are linked to the concentrations of reactants available, which increases linearly with pressure [1]. As a result, the pressure distribution across the active area of the fuel cell influences the local performance, and fuel cells with higher pressure over a significant fraction of the active area will see a corresponding increase in performance. Finally, the geometry of the flow field also has an effect on the ohmic losses since the geometry of the lands determines the shape of current paths, and contact resistance is affected by the total contact area. Consequently, if flow fields have significantly different land areas, this effect should also be considered.

The variations in the performance of fuel cells using different flow fields have mainly been attributed to their effectiveness at achieving uniform distributions, with little consideration given to the effects of the flow field's pressure characteristics. Achieving uniform distribution will improve the performance of the fuel cell without penalty to system performance. However, while a higher pressure drop will result in improved cell level performance, this comes at the expense of increasing pumping power. Higher inlet pressure will also necessitate using larger, more expensive auxiliary system components. Since the pressure effects trend in opposite directions, the net effect needs to be considered, as failure to consider either effect would yield erroneous results.

Based on the above observations, this paper focuses on the importance of decoupling the effects of pressure and distribution to achieve the proper performance comparisons of different PEMFC flow field designs. The effect of pressure on electrochemistry is first considered, and a thermodynamic First-Law analysis of a representative fuel cell supply system is developed in order to demonstrate how supply pressure affects the performance requirements of all components of an auxiliary system. Then, a method for estimating the

pressure contribution on fuel cell performance is developed. Finally, a comprehensive 3D computational model is used to simulate two different conventional flow field designs in order to demonstrate the method of decoupling pressure and distribution effects.

2. PRESSURE EFFECTS ON FUEL CELL PERFORMANCE AND AUXILIARY POWER

The rates of the electrochemical reactions in a fuel cell and therefore the amount of current produced by the fuel cell are sensitive to the temperature and concentration of the reacting species. Additionally, the protonic conductivity of the polymer electrolyte is largely a function of its water content. The water absorption of the membrane depends on relative humidity, so ohmic losses are affected by relative humidity. There is interplay between temperature, pressure and relative humidity and both experiments and computations have been performed to map the response of PEMFCs to variations in these operating parameters. Wang et al. [31] performed an experimental study on a PEMFC, in which the parametric dependence on operating temperature, pressure, and level of humidification were examined individually. It was observed that fuel cell power output increased monotonically with increasing pressure due to higher reactant concentrations supplied. The effects of temperature and humidity are linked: increase in cell temperature reduces the kinetic losses, but if the level of humidification is not sufficiently high, increase in temperature may also lead to drying of the membrane, reducing performance. It was shown that, if humidification is sufficient, performance increases monotonically with temperature. Furthermore, increase in humidification generally helps keep the electrolytic membrane hydrated. However, since water is also a product of fuel cell operation, very high inlet gas humidification may cause product water condensation and clogging of the porous GDL and channels, often referred to as “flooding”. Other studies, both experimental and computational, show the same trends [32, 33].

There are two ways that the pressure drop between inlet and outlet affects the performance and modeling of a fuel cell. Firstly, the current density produced by the electrochemical reactions is sensitive to the concentration of reacting species at the catalytic interface. The Tafel formulation of the Butler-Volmer equation [1, 34], which models electrochemical reactions, is

$$J = \zeta j_{ref} \left(\frac{[C_i]}{[C_{i,ref}]} \right)^{\gamma} exp\left(\frac{\alpha F \eta}{RT} \right). \tag{1}$$

where J is the volumetric current generation in the catalyst layer, ζ is the surface area to volume ratio of catalyst in the catalyst layer, j_{ref} is the reference area based current density for the catalyst, C_i and $C_{i,ref}$ are the actual and reference concentrations of the reacting species, γ is the concentration exponent which is often included for generality, α is the exchange coefficient, F is Faraday's constant, η is the activation overvoltage, and R and T are the universal gas constant and temperature.

Of particular interest to this discussion is the concentration term, $[C_i]$. The molar concentration of a species i in an ideal gas mixture is

$$[C_i] = P_i/(RT) \tag{2}$$

where P_i is the partial pressure. Inserting this expression into Equation 1 and holding all other quantities equal the current production at a set voltage is directly proportional to the local pressure, that is P^{γ}. Thus, any increase in local pressure would result in a proportional rise in local current production.

Secondly, the auxiliary system power requirements are directly affected by the required supply pressure of the inlet gases. A diagram of the basic thermodynamic devices required to supply one side (anode or cathode) of a fuel cell system with auxiliary heating and humidification is shown in Figure 1.

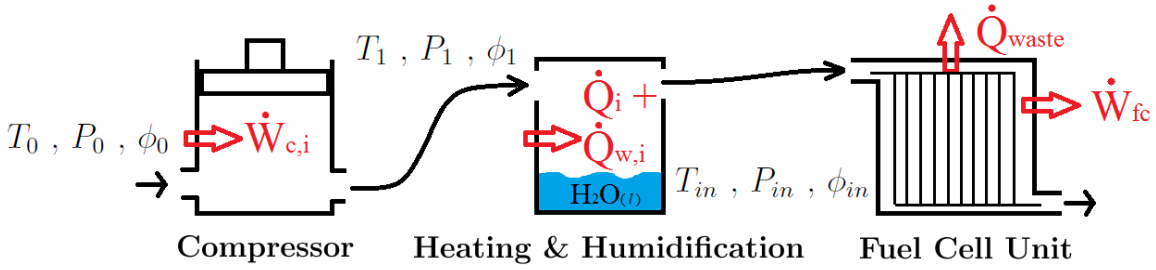

Figure 1. Diagram of the thermodynamic devices in a PEMFC system

The total energy cost of operating a fuel cell at desired inlet conditions can be calculated by finding the inputs required for each device shown in Figure 1 for both anode and cathode in order to bring supply gases from the local thermodynamic dead state (T_0, P_0, ϕ_0) to the desired inlet conditions (T_{in}, P_{in}, ϕ_{in}).

Assuming that a fuel cell is to be operated with a stoichiometry of ξ based on the operating current density j, at temperature T_{in}, pressure P_{in}, and relative humidity ϕ_{in}, and using the relationship between current produced by an electrochemical reaction and molar consumption rate of the reactants, the mass flow rate of dry gas may be determined by from,

$$\dot{m}_i = \frac{j A_{act} M_j}{Y_j n_j F} \xi \tag{3}$$

where the subscript i indicates either anode or cathode dry (un-humidified) gas mixture, and subscript j indicates the reactive species, either hydrogen for the anode or oxygen for the cathode. Y_j, is the mass fractions of hydrogen or oxygen in the dry supply gases, and n_j is the number of moles of electrons released per mole of reactant.

The power requirement for the compression process needed to bring the dry gas up to the inlet pressure may be obtained from

$$\dot{W}_{c,i} = \frac{1}{\eta_c} \dot{m}_i c_p T_0 \left(\left(\frac{P_{in}}{P_0} \right)^{\frac{k-1}{k}} - 1 \right) \tag{4}$$

which is derived for an ideal compression process and corrected for losses with the isentropic efficiency η_c. In Equation 12, c_p is the constant pressure specific heat, and k the ratio of specific heats of the gas being compressed. From isentropic relations and corrected for losses with isentropic efficiency, the temperature of the dry supply gas after compression may be derived as

$$T_1 = T_0\left[1 + \frac{\left(\left(\frac{P_{in}}{P_0}\right)^{\frac{k-1}{k}} - 1\right)}{\eta_c}\right]. \tag{5}$$

Additional heat may be required to raise the temperature of the compressed dry gas from intermediate temperature T_1 to the desired inlet temperature T_{in}, and this additional amount of heat, $\dot{Q}_i$, is given by

$$\dot{Q}_i = \dot{m}_i c_p (T_{in} - T_1). \tag{6}$$

From the definition of relative humidity the required mole fraction of water vapor, X_{H_2O}, in the humidified gas stream to achieve the desired relative humidity is calculated as

$$X_{H_2O} = \frac{\phi_{in} P_{v,in}}{P_{in}} \tag{7}$$

where $P_{v,in}$ is the saturation pressure of water vapor at the inlet temperature. The mass flow rate of water, $\dot{m}_{w,i}$, to attain the desired inlet relative humidity for either anode or cathode may then be found by using Equation 7 and assuming ideal gas mixture behavior, which results in

$$\dot{m}_{w,i} = \dot{m}_i\left(\frac{M_{H_2O}}{M_i}\right)\left(\frac{X_{H_2O}}{1 - X_{H_2O}}\right) \tag{8}$$

where X_{H_2O} is the mole fraction of water vapor, M is the molecular weight, and subscript i indicates the dry gas for either anode or cathode. The total mass flow rate supplied to the fuel cell anode or cathode is $\dot{m}_{tot} = \dot{m}_i + \dot{m}_{w,i}$.

The heat required for evaporating liquid water to achieve the desired relative humidity, $\dot{Q}_{w,i}$ may be approximated by using the enthalpy of vaporization of water, h_{fg}, at the inlet temperature

$$\dot{Q}_{w,i} = \dot{m}_{w,i} h_{fg}. \tag{9}$$

Due to the large enthalpy of vaporization of water, the energy required for the phase change is much larger than the sensible enthalpy change associated with heating, so the sensible enthalpy is ignored here. The total power requirement for the auxiliary system for either anode or cathode side, $\dot{W}_{aux,i}$, is then the sum of the power supplied for each process, i.e.

$$\dot{W}_{aux,i} = \dot{W}_{c,i} + \dot{Q}_i + \dot{Q}_{w,i}. \tag{10}$$

This analysis my be performed for both supply gases at the anode and cathode, and the total auxiliary system power is then the sum of the power required to pre-treat both sides.

In addition to the direct effect on the auxiliary power requirement that pressure drop imposes, there is another, more subtle effect which also needs to be considered, particularly in computational modeling. When testing a fuel cell experimentally, humidification temperature and pressure are set for the desired operating point in order to control the inlet relative humidity. However, in a numerical simulation, where the inlet species fractions must be set by the user, particular care must be taken. Noting in Equation 7 that the required species fraction of water to achieve a desired inlet relative humidity is a function of both temperature and pressure when calculating the species fraction for the inlet boundary conditions, the correct *local* temperature and pressure must be used. Since the required species fraction of water to achieve a fixed relative humidity is inversely proportional to total pressure (Eq. 7), if the outlet pressure is used to calculate the inlet species fractions for a design with an appreciable pressure drop, the actual inlet relative humidity could be significantly off, and may even be physically impossible (i.e. $\phi > 100\%$).

The supply rates of dry hydrogen and air are fixed by setting the operating stoichiometry, but the total mass flow rate will vary with relative humidity. Note that while this analysis assumes the dry hydrogen to initially be at ambient conditions for the sake of calculating the energy cost of operation, hydrogen would be stored at high pressure and would be throttled to the desired inlet pressure in reality. For an inlet pressure that is close to atmospheric pressure and at typical fuel cell operating temperatures and relative humidities, the mole fraction of water vapor can easily make up 25-35% of the mass supplied to the cathode, and with the low molecular weight of hydrogen, 60% or more of the mass for the anode. Therefore, incorrectly specified mass flow rates and species fractions at the inlet can have a significant effect on the performance modeling of the fuel cell itself. Additionally, the inlet pressure not only affect the compressor work in the auxiliary system, but through its effect on the mixture species fractions will also affect the energy requirements of the humidification process, which can be quite significant due to the large enthalpy of vaporization of water.

In order to account for all of these effects, the outlet pressure may not be used as a representative pressure for the entire fuel cell domain for designs with a significant pressure drop. Instead, *it is proposed that all of the inlet conditions be fixed between fuel cell designs in order to make a more equitable comparison.* Thus, the design with the naturally lower pressure loss should have the outlet pressure boundary condition raised such that the inlet pressures between compared designs are the same. This results in all fuel cells under consideration having supply gases at the same thermodynamic state, and the total auxiliary system power for each cell being identical. While it may not be common practice to operate a fuel cell with a restriction at the outlet to increase cell pressure, this is done here solely for the sake of comparing the performance of the flow fields.

Fixing the state of the supply gases simultaneously eliminates the differences in total system performance that would arise from all of the pressure effects, both on auxiliary power requirements and fuel cell unit performance. The difference in the observed performance

of the fuel cell units may then be attributed solely to the flow field's effectiveness at reactant distribution. The relative influence of pressure and reactant distribution on the performance of the two flow fields may then be determined by comparison of the performance results obtained by using fixed outlet pressures compared to those obtained using fixed inlet properties.

Additionally, if results have been obtained for different flow fields without accounting for the different inlet pressures, some insight into the relative pressure effect may be gained by examining Equation 1. Holding all quantities constant on the right hand side of Equation 1 except for the concentration term, C_i, is the equivalent to supplying the same inlet mixtures and operating conditions with the exception of different inlet pressures. Then the current density produced at a fixed voltage, and thus the power density, becomes a function of concentration only. Isolating the concentration term and applying the Ideal Gas Law and Dalton's Law of Partial Pressures, the following equation can be obtained;

$$\left(\frac{[C_i]}{[C_{i,ref}]}\right)^{\gamma} = \left(\frac{P_{in}X_i/RT}{P_{ref}/RT}\right)^{\gamma}. \tag{11}$$

Because the mixture properties are held constant in this comparison, the terms X_i, R, and T are constants. The following equation, in which $\hat{P}$ represents the total inlet pressure normalized by ambient pressure as a reference, can be used as a metric to estimate the relative pressure effect between designs.

$$\dot{W}_{fc} \propto \hat{P}^{\gamma} = \left(\frac{P_{in}}{P_0}\right)^{\gamma} \tag{12}$$

Note that using Equation 12 to estimate pressure effects does not account for the difference in auxiliary system power requirements, and does not capture the effect of different species fractions in the supply gases due to the humidity variation with pressure. Therefore,

the proposed method of fixing inlet properties for comparison is the recommended method. However, Equation 12 may be used to gain some insight into the relative effect of pressure in previously published results where these effects were not considered.

3. COMPUTATIONAL METHODS

3.1. Mesh and Model Settings. The commercial software package ANSYS Fluent 15.0 was used to perform a computational study on the performance of fuel cells with different flow field designs using the PEMFC Add-On Module. The Serpentine and Parallel flow field designs were selected for this study, as they are among the most well-documented flow field designs, both computationally and experimentally, and are often used as benchmark designs [4, 6, 7, 9–12, 15–18, 22, 24, 25, 27, 28, 30, 32, 33, 35–38]. Furthermore, the present authors have experimentally validated CFD results for the serpentine and parallel-in-series flow field designs in previous work [15, 16] using the same software package, and the computational study performed for the present work was based on the same model parameters. These designs were chosen to demonstrate the importance of the proposed method of comparison, but the same methods may be used for any flow field geometry.

The active area of each fuel cell was square and the geometry specifications of the designs are listed in Table 2. The geometries were meshed with the ANSYS Workbench 15.0 Meshing application. After several iterations of both mesh quality and fineness to ensure stable convergence and mesh independence, the final meshes for both designs contained approximately 1.8 million nodes using hexahedral cells with an orthogonal quality of 0.999 or greater. The maximum mesh size was set to 0.25 mm, which was the spacing in the in-plane direction for all layers. The spacing in the through-plane direction was varied as necessary in order to fit cells within the thinner layers. The channel layer had 6 cells across, and all other layers were 4 cells across, as can be seen in the Figure 4 that shows the through plane mesh spacing.

Table 2. Fuel cell geometry parameters for parallel and serpentine fuel cells

Geometry Parameter	**Value**
Active Area	25.0 cm^2
Number of Channels	25
Channel Area- Serpentine	51.0 %
Channel Area- Parallel	53.0 %
Total BPP Thickness	2.50 *mm*
Channel Depth	1.50 *mm*
Channel Width	1.00 *mm*
Rib Width	1.00 *mm*
GDL Thickness	0.35 *mm*
Catalyst Thickness	0.01 *mm*
Electrolyte Thickness	0.15 *mm*
Total Cell Thickness	5.87 *mm*

In addition to the usual mass, momentum, energy, and species conservation equations solved in CFD modeling, additional joule heating, reaction heating, electrochemistry sources, Butler-Volmer rate, and multiphase models, along with electrical potential and electronic and protonic conduction are solved to simulate fuel cell performance. It should be noted that two phase flow for condensed water vapor is not fully simulated here, but rather the assumption is made that the water vapor travels with the free stream velocity in the channel layer as a fine mist. The effect of poor blockage in the porous zones (GDL and Electrolyte) is approximated by multiplying the porosity by $(1 - s)$, where s is the volume fraction of liquid water. For model details, the reader is referred to [39].

For these simulations, the SIMPLE (Semi-Implicit Method with Pressure Linked Equations) solver was used, with least squares cell based gradient, while the discretization set to standard for pressure and second-order upwind for all other parameters. The thermal boundary condition for the exterior walls was set to a constant temperature of 348 K. The modeling parameters which were common to all runs in the simulations are given in Table 3 with references to indicate the source of critical parameters. Mass flow boundary conditions were used for both anode and cathode inlets with a temperature of 348 K, and pressure boundary conditions were used for the outlets. The inlet mass flow rates were

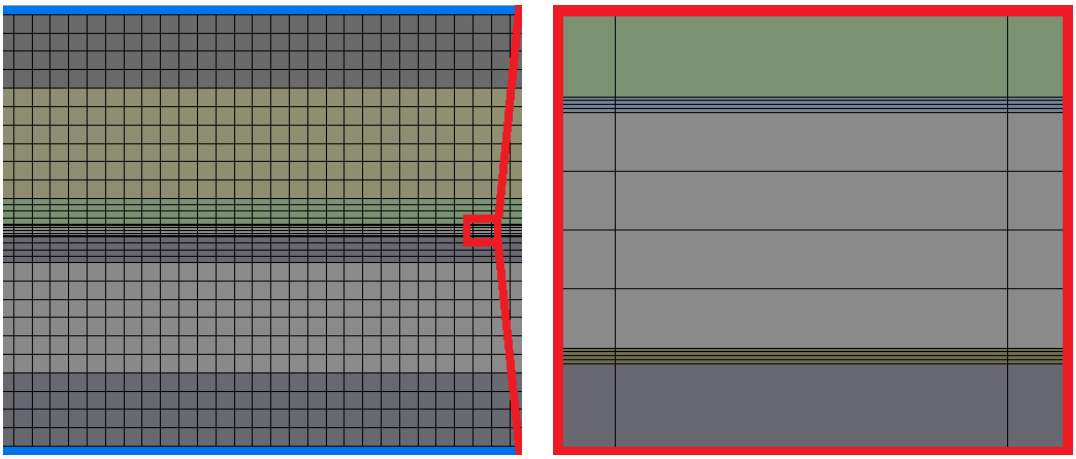

(a) Cross section - all sayers (b) Details of catalyst and electrolyte sayers

Figure 2. (a) Cut view of all through plane mesh layers and (b) enlargement of red insert in (a) showing catalyst and electrolyte layer details (color version available online)

constant for all operating points, and were calculated such that the stoichiometry would be 2 at a current density of 2 A/cm^2, ensuring that the amount of dry hydrogen and dry air stayed constant between all runs. However, species fractions, and therefore total mass flow rates, as noted in the previous section, are dependent on the inlet pressure required for each design. Consequently, they were not constant between all runs since there were different amounts of water vapor present to attain the same relative humidity at different pressures. The pressure drops across the fuel cell for the Parallel and Serpentine designs were quite different, thus different inlet mole fractions of water vapor were required for the same relative humidity.

3.2. Simulation Strategy. For each design, simulations were run with potentiostatic boundary conditions at points from 0.85 V to 0.15 V at 0.1 V increments to obtain polarization and power density curves. Both the Parallel and Serpentine designs were first simulated with the outlet pressure boundary condition set to 0 Pa gage, and the inlet species fractions calculated for the desired relative humidity at atmospheric pressure. The inlet total pressure of the Parallel design deviated from atmospheric pressure by less than 1%, which did not significantly affect the water mole fraction required to attain the desired relative

Table 3. Numerical model parameters used in the fluent simulations

Model Parameter	**Units**	**Values**
Ref. Current Density- Anode	A/m^3	4.48E+05 [15]
Ref. Current Density- Cathode	A/m^3	4.48 [15]
Catalyst Layer Surface to Volume Ratio	m^{-1}	1.25e+07 [15]
Ref. Concentration- Anode	$kmol/m^3$	1.0
Ref. Concentration- Cathode	$kmol/m^3$	1.0
Concentration Exponent- Anode		1.0
Concentration Exponent- Cathode		1.0
Exchange Coefficient- Anode		1.0 [15]
Exchange Coefficient- Cathode		1.0 [15]
Open Circuit Voltage	$Volt$	1.0
Leakage Current	A	0.0
Reference Diffusivity- H_2	m^2/s	8.0E-05 [15]
Reference Diffusivity- O_2	m^2/s	2.0E-05 [15]
Reference Diffusivity- H_2O	m^2/s	5.0E-05 [15]
Saturation Exponent (Pore Blockage)		2.0 [36]
Temperature (Boundaries and Inlet)	K	348 [15]
Relative Humidity- Cathode	%	75
Relative Humidity- Anode	%	100

humidity. The boundary conditions for the zero back pressure Parallel run are listed in Table 4. The Serpentine design, however, has a significantly higher inlet pressure, and the species fraction of water calculated for the desired relative humidity at atmospheric pressure is not physically attainable at the real inlet pressures for both anode and cathode, as those mole fractions of water vapor would result in greater than 100% relative humidity. Using the inlet pressures obtained by the initial results, the inlet species fractions and total mass flow rates were recalculated, and the serpentine design was run again. The slight change in mass flow rate resulted in a corresponding change in inlet pressure, and this iterative process was carried out once more to determine the correct species fractions, and the final values are given in Table 4. Finally, the Parellel design was run again, this time with the outlet pressure boundary conditions set such that the inlet pressures would be the same as the Serpentine

design, and using the same mixture fractions and mass flow rate as the serpentine design. In this way, the two designs can be compared using the proposed method, with the supply gases in identical states and therefore with identical auxiliary loads.

Table 4. Numerical model parameters affected by inlet pressure

Model Parameter	Units	Values
Parallel- Zero Back Pressure		
Inlet Pressure- Anode	$Pa, gage$	0
Mass Flow Rate- Anode	kg/s	6.65E-06
Hydrogen Mole Fraction		0.625
Water Mole Fraction- Anode		0.375
Inlet Pressure- Cathode	$Pa, gage$	0
Mass Flow Rate- Cathode	kg/s	4.43E-05
Oxygen Mole Fraction		0.15094
Water Mole Fraction- Cathode		0.28125
Serpentine Zero Back Pressure and Parallel Pressure Matched		
Inlet Pressure- Anode	$Pa, gage$	5000
Mass Flow Rate- Anode	kg/s	5.964E-06
Hydrogen Mole Fraction		0.65497
Water Mole Fraction- Anode		0.34503
Inlet Pressure- Cathode	$Pa, gage$	32000
Mass Flow Rate- Cathode	kg/s	4.1648E-05
Oxygen Mole Fraction		0.16511
Water Mole Fraction- Cathode		0.21374

3.3. Convergence Criteria. In determining the point at which the solution is considered to have converged, it was necessary to look further than the standard method of residuals reduction when using the PEMFC Module. It was found that species and current conservation would not be satisfied until several thousand iterations after apparent convergence was achieved based solely on the residuals, as noted in [40]. Naturally, current and species conservation are more relevant and accordingly a better indicator of simulation

convergence than the residuals. The coupled current and species models were the slowest to converge, therefore total current and species values were monitored directly in order to ensure convergence.

The current produced by the electrochemical reactions of hydrogen and oxygen may be determined by

$$I_{O_2} = \frac{4F}{M_{O_2}} \Delta \dot{m}_{O_2}, \tag{13}$$

$$I_{H_2} = \frac{2F}{M_{H_2}} \Delta \dot{m}_{H_2}. \tag{14}$$

The total current at the terminals and mid-plane of the fuel cell (Cathode, Anode, and Electrolyte Currents), as well as the rate of hydrogen and oxygen consumption due to electrochemical reactions ($\Delta \dot{m}_{H_2}$ and $\Delta \dot{m}_{O_2}$) were monitored. Using the species consumption rates, the expected current production was calculated using Equations 10 and 11. When all of these values agreed to within 1%, the solution was considered to have converged. Figure 5 shows a representative convergence graph where the predicted total current and species currents are plotted against iteration count.

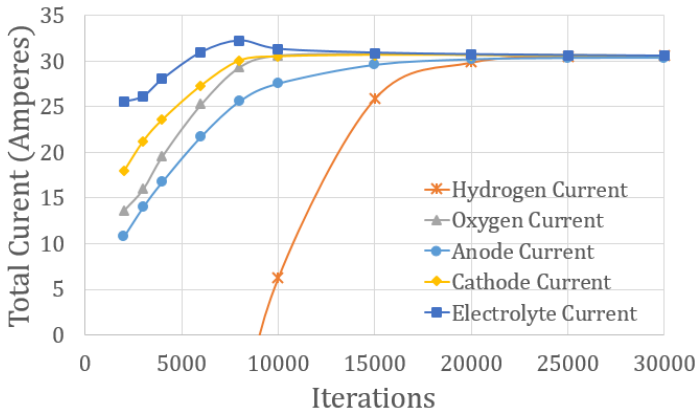

Figure 3. Convergence plot of species and current for parallel design at 0.25 V

If the simulation is stopped prematurely based on monitoring residuals only, apparent results may be obtained, but they would not be reliable as the currents at different planes in the fuel cell do not agree. Additionally, the species data, which is of particular interest for this work, is the last to converge, taking even longer to fall within the set convergence tolerance than the measured current values, as can be seen in Figure 5. Even monitoring the current data directly would not be enough, because the hydrogen data would still not satisfy the coupled mass conservation and electrochemistry models. Thus, it is imperative to monitor all of the quantities associated with the electrochemistry models for convergence criteria.

4. RESULTS AND DISCUSSION

The Serpentine and Parallel designs were simulated using the methods and settings described above. Even though a fixed mass flow rate was used for all operating points, the pressure drop varied slightly with the current density level for each design. This was because the rate of species consumption and mixture properties changed with the electrochemical reaction rate, but the variation in pressure drop was slight. It was found that, with the operating conditions used in this study, the Parallel design had an inlet gage pressure of approximately 70 Pascals on the anode side, and 650 Pascals on the cathode side, while for the Serpentine design, the anode inlet gage pressure was approximately 5,000 Pascals, and the cathode 32,000 Pascals. Relative to standard atmospheric pressure, the anode and cathode inlets for the Parallel design had a difference of only 0.06% and 0.6% respectively, while the Serpentine anode and cathode deviated from atmospheric pressure by 4.9% and 31.6%, respectively. The polarization and power density curves obtained in these simulations are given in Figure 4.

Figure 4 clearly indicates that the zero back pressure Serpentine design outperforms the Parallel design at both back pressures in the high current density range. If the polarization curves of both designs with zero back pressure were compared directly then the effects of

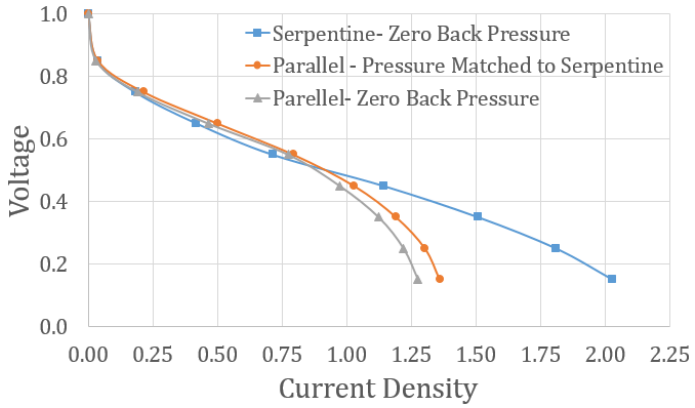

(a) Polarization curves

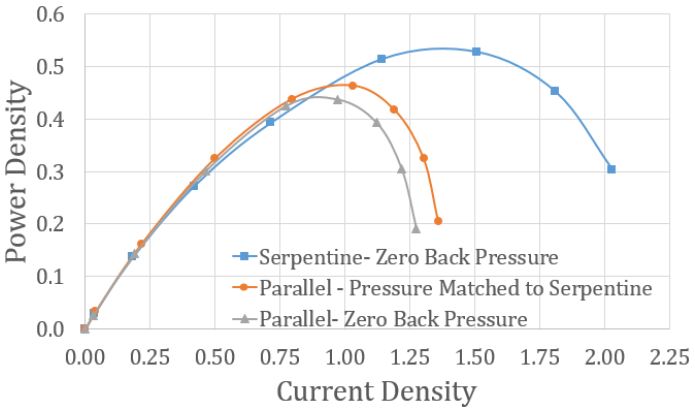

(b) Power density curves

Figure 4. Comparison of performance for serpentine and parallel designs (a) polarization curves, and (b) power density curves

the different inlet pressures, both on the fuel cell itself and on the auxiliary power, would be overlooked. One could perform the analysis derived in Section 2 for both designs and adjust the power density curves accordingly. However, by raising the back pressure of the parallel design so as to match the inlet pressure to that of the serpentine designs, this analysis was not required. By matching inlet conditions, the reactant gases were supplied at identical states to both designs so the fuel cells received identical inputs, while the auxiliary systems had identical loads. Thus, the effects of the different pressure drop of the two designs have been effectively negated. The modes of mass transport remain unchained though, so any remaining difference in performance will be due to the mass transport properties of the flow

Table 5. Performance comparison using traditional and proposed methods

Run	**Peak Power Density** (W/cm^2)	**Difference** (%)
Serpentine, Zero Back Pressure	0.527	0.0
Parallel, Zero Back Pressure	0.437	17.1
Parallel, Inlet Pressure Matched	0.463	12.2

fields. As noted in Section 1, the channel and rib geometry can affect the ohmic contact resistance if there are significant differences in the designs, however the land areas of these two designs were very similar (See Tab. 2) and so any difference in ohmic contact resistance should be negligible.

By comparing the two results obtained for the parallel design, the relative effects of pressure and mass transport characteristics may be estimated. The peak power density in each run, and the performance relative to the Serpentine design are given in Table 5. When the difference in performance due to the higher supply pressure of the Serpentine design was removed by making the comparison with identical inlet properties, the discrepancy between the peak performance of the Parallel design and the Serpentine design was reduced from 17.1 % to 12.2 %. Consequently it might be reasoned that the superior mass transport characteristics of the serpentine design yielded a 12.2 % performance increase over the parallel design, and the effects of the increased supply pressure due to the serpentine's higher pressure loss produced an additional 4.9 % performance increase.

The individual effects of pressure and distribution on performance enhancement were further observed by examining the concentration and reactant gas velocity in each design at the level of the catalyst layer. The contour plots of computed molar concentration of oxygen and velocity at the cathode GDL-catalyst interface are given in Figure 5, and the average and maximum molar concentrations of oxygen, and mixture velocity magnitudes for all cases are given in Table 6. The maximum molar concentration of reactant, oxygen for the cathode side, is limited by the molar concentration supplied at the inlet, and the maximum oxygen concentration for all three designs occurs near the inlet, as can be seen

in Figure 5. The limiting maximum concentration will be determined by the inlet pressure and mole fraction of oxygen (Eq. 2), which both have been noted to be directly affected by the pressure drop. The maximum concentration at the catalyst layer should follow the supply concentration. Since the serpentine and inlet pressure matched parallel designs have an inlet pressure approximately 30 % higher than the zero back pressure parallel design, as well as a slightly higher inlet mole fraction of oxygen due to the relative humidity effect, it would be expected that the maximum concentration should be slightly over 30 % higher in these designs. Furthermore, it would be expected that the serpentine and pressure matched parallel cases would have a similar maximum oxygen concentration. From Table 6 it can be seen that the higher inlet pressure designs have a maximum concentration approximately 37 % higher than the zero back pressure parallel, and the serpentine and pressure matched parallel designs only differ by 2.6 %, both in the expected ranges.

Table 6. Oxygen concentration and mixture velocities at the cathode GDL-Catalyst interface

Run	O_2 Avg.	O_2 Max.	V Avg.	V Max.
	$kmol\ m^{-3}$		$m\ s^{-1}$	
Serpentine, Zero Back Pressure	2.54e-3	6.48e-3	9.76e-3	3.09e-2
Parallel, Zero Back Pressure	8.47e-4	4.71e-3	1.41e-3	4.37e-3
Parallel, Inlet Pressure Matched	1.26e-3	6.65e-3	9.71e-4	2.67e-3

The average oxygen concentration over the catalyst layer in the pressure matched parallel design is higher than that in the parallel design with zero back pressure, but still does not reach the same level as the serpentine design. This difference in concentration accounts for the 5 % performance difference between the two parallel cases, relative to the serpentine case. The further increase in average concentration in the serpentine design may be attributed to the enhanced mass transport mechanism. As has been noted by Feser et al. [10], there is some degree of convective transport in the Serpentine design which enhances mass transport from the channels to the catalyst layer. This is clearly evident in the

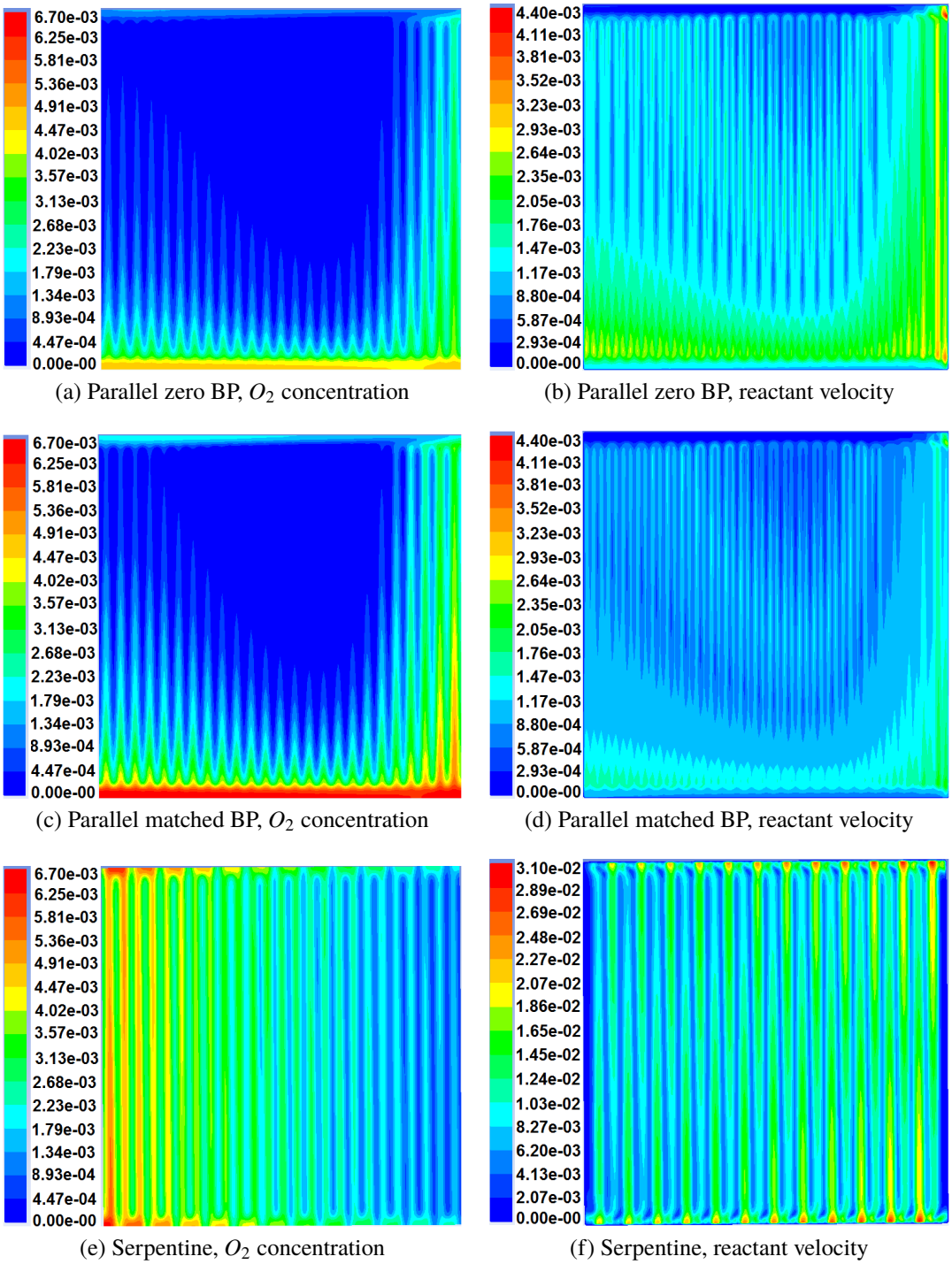

(a) Parallel zero BP, O_2 concentration

(b) Parallel zero BP, reactant velocity

(c) Parallel matched BP, O_2 concentration

(d) Parallel matched BP, reactant velocity

(e) Serpentine, O_2 concentration

(f) Serpentine, reactant velocity

Figure 5. Contours of oxygen molar concentration ($kmol/m^3$) and velocity magnitude (m/s) at the cathode GDL-catalyst interface, at 0.35 V for the serpentine design, and parallel design at both back pressures (inlets at bottom left, color version available online)

velocity contours in Figure 5, where the pattern of higher gas velocity under ribs of adjacent channels which are far from a u-bend is easily visible. Note that the scale of the velocity at the catalyst layer in the Serpentine design is an order of magnitude larger than that in the two Parallel designs which are of similar order (Tab. 6). This enhanced transport mechanism accounts for the remaining 12 % performance increase over the Parallel design. However, this performance enhancement comes at a cost, as large pressure gradients are required in order to achieve some degree of convective flow through the porous GDL material.

In the case of comparison of the parallel and serpentine designs presented here, the ranking of performance was not altered when the proposed comparison method was utilized, but the apparent gap in performance was narrowed. Since the supply gases are at identical states, there is no difference in auxiliary power between designs, thus it is appropriate to compare the polarization curves with the same inlet state directly. If the difference in performance between competing designs is not as great as that between the parallel and serpentine designs, or if the relative difference in pressure is large, failure to decouple the pressure and distribution effects while directly comparing the polarization curves may result in more significant differences. This is an important consideration for fuel cell designers because, in some applications, constraints such as total system mass, volume, or capital cost can be critical restrictions, thus a design with lower peak power density, but which demands a smaller auxiliary system may still be desirable over a higher power density design which has more stringent auxiliary system demands.

In addition to demonstrating the method of decoupling pressure and distribution effects, results from previous studies may also be examined to emphasize the importance of doing so. Catlin et al. [28] conducted an optimization study on the geometry of the serpentine flow field. While the proposed method of fixing inlet conditions was not used, the authors did account for pumping power in their calculation of net power, and noted that the designs under consideration differed in order when ranked by net as opposed to gross power. Han et al. [41] presented both experimental and computational results for

a PEMFC operating with different-geometry flow distributors by adding wave-like surface designs at the cathode channels in a Multi-Serpentine flow field. Relative to the reference case of smooth channels, the authors reported that the best performer had a power increase of 5.76 % from their experimental results, but also had an increase in the inlet gage pressure from approximately 4 kPa to 16 kPa. The authors commented on the fact that increased pressure was undesirable due to the increase in pumping requirements; however, the difference in performance between the designs was attributed solely to changes in mass transport characteristics. Using the normalized inlet pressure method given by Equation 12, with the concentration exponent of $\gamma = 0.5$ used in [41], the contribution of increased pressure can be estimated. Based on the reported reference case (smooth bottom) with the normalized inlet gage pressure of $\hat{P}_{base} = 1.0395$ and the best performer case with the normalized inlet pressure of $\hat{P}_{case1} = 1.1579$, the predicted percentage increase in performance due to increased pressure is 5.5 %. This value almost perfectly matches the reported increase in performance over the reference case, and so the dominating mechanism for performance enhancement is, in fact, increased operating pressure. This implies that the same performance increase may be realized by increasing the outlet pressure of the simpler smooth bottomed Multi-Serpentine design, thereby rendering the more complicated geometry with wave-like structures in the channels unnecessary.

5. SUMMARY AND CONCLUSIONS

A comprehensive method for comparing the performance of PEMFCs at a system level has been proposed. This method decouples the effects of reactant distribution and pressure drop due to flow distributor design on the fuel cell, and normalizes auxiliary power between designs for comparison of overall performance. This provides researchers and fuel cell developers a tool to better rank and select flow distributor designs. The computational modeling and necessary equations required to account for these effects were first presented. The proposed method was then computationally implemented on two well-

known traditional flow distributor designs, Parallel and Serpentine. Additionally, a metric for approximating the relative effects of pressure in previously obtained results that do not employ the proposed method of fixing inlet conditions was proposed and demonstrated. It was shown that the contribution to performance caused by pressure drop across different flow distributor designs, which is usually considered negligible compared to distribution effects, had a significant impact on the fuel cell performance. The comparison of the Parallel and Serpentine design yielded a 17.1 % total difference in peak power density when both had the same outlet pressure, but 4.9 % was shown to be due to the pressure effects while the remaining 12.2 % was due to distribution effects. Furthermore, in examination of prior works, it was found that, in some instances, the pressure effect can be the primary contributor to the observed difference in fuel cell performance. These results demonstrate that the effect of pressure, both on the auxiliary system and the fuel cell itself, could be a significant contributor to performance, and should not be ignored when considering flow distributor designs that induce significant pressure drops. Because the effects of enhanced distribution are only beneficial, while increased pressure drop tends to both increase cell performance and auxiliary power requirements, thus causing both positive and negative impacts on system performance, the ability to decouple these two effects is of critical importance when comparing the relative attributes of multiple flow field designs.

ACKNOWLEDGMENTS

This work was supported by the National Science Foundation under the grant No. CMMI-1131659, and by the Missouri University of Science and Technology's Innovation Initiative.

REFERENCES

[1] R. O'Hayre, S.-W. Cha, W. Colella, F. B. Prinz, Fuel Cell Fundamentals, 2nd Edition, John Wiley & Sons, 2009.

[2] N. Muradov, Emission-free fuel reformers for mobile and portable fuel cell applications, Journal of Power Sources 118 (1-2) (2003) 320–324. doi:10.1016/S0378-7753(03)00078-8.

[3] S. E. Wright, Comparison of the theoretical performance potential of fuel cells and heat engines, Renewable Energy 29 (2) (2004) 179–195. doi:10.1016/S0960-1481(03)00191-5.

[4] H.-W. Wu, A review of recent development: Transport and performance modeling of PEM fuel cells, Applied Energy 165 (2016) 81–106. doi:10.1016/j.apenergy.2015.12.075.
URL http://linkinghub.elsevier.com/retrieve/pii/S0306261915016487

[5] J. Wang, Theory and practice of flow field designs for fuel cell scaling-up: A critical review, Applied Energydoi:10.1016/j.apenergy.2015.01.032.
URL http://linkinghub.elsevier.com/retrieve/pii/S0306261915000380

[6] A. P. Manso, F. F. Marzo, J. Barranco, X. Garikano, M. Garmendia Mujika, Influence of geometric parameters of the flow fields on the performance of a PEM fuel cell. A review, International Journal of Hydrogen Energy 37 (20) (2012) 15256–15287. doi:10.1016/j.ijhydene.2012.07.076.
URL http://dx.doi.org/10.1016/j.ijhydene.2012.07.076

[7] J. Wang, H. Wang, Flow-field designs of bipolar plates in PEM fuel cells: Theory and applications, Fuel Cells 12 (6) (2012) 989–1003. doi:10.1002/fuce.201200074.

[8] J. Wang, H. Wang, Discrete approach for flow field designs of parallel channel configurations in fuel cells, International Journal of Hydrogen Energy 37 (14) (2012) 10881–10897. doi:10.1016/j.ijhydene.2012.04.034.
URL http://dx.doi.org/10.1016/j.ijhydene.2012.04.034

[9] T. V. Nguyen, A Gas Distributor Design for Proton-Exchange-Membrane Fuel Cells, Journal of The Electrochemical Society 143 (5) (1996) L103. doi:10.1149/1.1836666.

[10] J. P. Feser, a. K. Prasad, S. G. Advani, On the relative influence of convection in serpentine flow fields of PEM fuel cells, Journal of Power Sources 161 (1) (2006) 404–412. doi:10.1016/j.jpowsour.2006.04.129.

[11] H.-C. Chiu, J.-H. Jang, W.-M. Yan, H.-Y. Li, C.-C. Liao, A three-dimensional modeling of transport phenomena of proton exchange membrane fuel cells with various flow fields, Applied Energy 96 (2012) 359–370. doi:10.1016/j.apenergy.2012.02.060.
URL http://dx.doi.org/10.1016/j.apenergy.2012.02.060

[12] Y. Vazifeshenas, K. Sedighi, M. Shakeri, Numerical investigation of a novel compound flow- field for PEMFC performance improvement, International Journal of Hydrogen Energy 40 (43) (2015) 15032–15039. doi:10.1016/j.ijhydene.2015.08.077.
URL http://dx.doi.org/10.1016/j.ijhydene.2015.08.077

[13] D. Juarez-Robles, A. Hernandez-Guerrero, B. Ramos-Alvarado, F. Elizalde-Blancas, C. E. Damian-Ascencio, Multiple concentric spirals for the flow field of a proton exchange membrane fuel cell, Journal of Power Sources 196 (19) (2011) 8019–8030. doi:10.1016/j.jpowsour.2011.05.029.
URL http://dx.doi.org/10.1016/j.jpowsour.2011.05.029

[14] N. Guo, M. C. Leu, U. O. Koylu, Network based optimization model for pin-type flow field of polymer electrolyte membrane fuel cell, International Journal of Hydrogen Energy 38 (16) (2013) 6750–6761. doi:10.1016/j.ijhydene.2013.03.066.
URL http://dx.doi.org/10.1016/j.ijhydene.2013.03.066

[15] N. Guo, M. C. Leu, U. O. Koylu, Bio-inspired flow field designs for polymer electrolyte membrane fuel cells, International Journal of Hydrogen Energy 39 (36) (2014) 21185–21195. doi:10.1016/j.ijhydene.2014.10.069.
URL http://linkinghub.elsevier.com/retrieve/pii/S0360319914029097

[16] B. P. Saripella, U. O. Koylu, M. C. Leu, Experimental and Computational Evaluation of Performance and Water Management Characteristics of a Bio-Inspired Proton Exchange Membrane Fuel Cell, Journal of Fuel Cell Science and Technology 12 (6). doi:10.1115/1.4032041.

[17] E. Birgersson, M. Vynnycky, A quantitative study of the effect of flow-distributor geometry in the cathode of a PEM fuel cell, Journal of Power Sources 153 (1) (2006) 76–88. doi:10.1016/j.jpowsour.2005.03.211.

[18] F. Arbabi, R. Roshandel, An Innovative Three Dimensional Numerical Model for Bipolar Plates to Enhance the Efficiency of PEM Fuel Cells (2012) 1–10doi:10.1115/FuelCell2012-91142.

[19] M. Grujicic, C. L. Zhao, K. M. Chittajallu, J. M. Ochterbeck, Cathode and interdigitated air distributor geometry optimization in polymer electrolyte membrane (PEM) fuel cells, Materials Science and Engineering B: Solid-State Materials for Advanced Technology 108 (3) (2004) 241–252. doi:10.1016/j.mseb.2004.01.005.

[20] A. D. Santamaria, N. J. Cooper, M. K. Becton, J. W. Park, Effect of channel length on interdigitated flow-field PEMFC performance: A computational and experimental study, International Journal of Hydrogen Energy 38 (36) (2013) 16253–16263. doi:10.1016/j.ijhydene.2013.09.081.
URL http://dx.doi.org/10.1016/j.ijhydene.2013.09.081

[21] H.-C. Liu, W.-M. Yan, X.-D. Wang, Effects of Flow Channel Area Ratio on Local Transport Characteristics and Cell Performance of 3D PEMFCs, Journal of The Electrochemical Society 154 (12) (2007) B1338. doi:10.1149/1.2789349.

[22] X. D. Wang, Y. Y. Duan, W. M. Yan, X. F. Peng, Effects of flow channel geometry on cell performance for PEM fuel cells with parallel and interdigitated flow fields, Electrochimica Acta 53 (16) (2008) 5334–5343. doi:10.1016/j.electacta.2008.02.095.

[23] V. Thitakamol, A. Therdthianwong, S. Therdthianwong, Mid-baffle interdigitated flow fields for proton exchange membrane fuel cells, International Journal of Hydrogen Energy 36 (5) (2011) 3614–3622. doi:10.1016/j.ijhydene.2010.12.060.
URL http://dx.doi.org/10.1016/j.ijhydene.2010.12.060

[24] C. T. Wang, Y. C. Hu, P. L. Zheng, Novel biometric flow slab design for improvement of PEMFC performance, Applied Energy 87 (4) (2010) 1366–1375. doi:10.1016/j.apenergy.2009.05.039.
URL http://dx.doi.org/10.1016/j.apenergy.2009.05.039

[25] B. Lee, K. Park, H.-m. Kim, Numerical Optimization of Flow Field Pattern by Mass Transfer and Electrochemical Reaction Characteristics in Proton Exchange Membrane Fuel Cells 8 (2013) 219–234.

[26] X.-D. Wang, Y.-Y. Duan, W.-M. Yan, Numerical study of cell performance and local transport phenomena in PEM fuel cells with various flow channel area ratios, Journal of Power Sources 172 (1) (2007) 265–277. doi:10.1016/j.jpowsour.2007.07.026.

[27] H. Liu, P. Li, K. Wang, Optimisation of pem fuel cell flow channel dimensions - mathematic modeling analysis and experimental verification, International Journal of Hydrogen Energy 38 (23) (2013) 9835–9846. doi:10.1016/j.ijhydene.2013.05.159.
URL http://linkinghub.elsevier.com/retrieve/pii/S0360319913013918

[28] G. Catlin, S. G. Advani, A. K. Prasad, Optimization of polymer electrolyte membrane fuel cell flow channels using a genetic algorithm, Journal of Power Sources 196 (22) (2011) 9407–9418. doi:10.1016/j.jpowsour.2011.06.073.
URL http://dx.doi.org/10.1016/j.jpowsour.2011.06.073

[29] M. Grujicic, K. M. Chittajallu, Optimization of the cathode geometry in polymer electrolyte membrane (PEM) fuel cells, Chemical Engineering Science 59 (24) (2004) 5883–5895. doi:10.1016/j.ces.2004.07.045.

[30] Y. M. Ferng, A. Su, A three-dimensional full-cell CFD model used to investigate the effects of different flow channel designs on PEMFC performance, International Journal of Hydrogen Energy 32 (17) (2007) 4466–4476. doi:10.1016/j.ijhydene.2007.05.012.

[31] L. Wang, H. Liu, Performance studies of PEM fuel cells with interdigitated flow fields, Journal of Power Sources 134 (2) (2004) 185–196. doi:10.1016/j.jpowsour.2004.03.055.

[32] W.-M. Yan, C.-H. Yang, C.-Y. Soong, F. Chen, S.-C. Mei, Experimental studies on optimal operating conditions for different flow field designs of PEM fuel cells, Journal of Power Sources 160 (1) (2006) 284–292. doi:10.1016/j.jpowsour.2006.01.031.

[33] J. P. Kloess, X. Wang, J. Liu, Z. Shi, L. Guessous, Investigation of bio-inspired flow channel designs for bipolar plates in proton exchange membrane fuel cells, Journal of Power Sources 188 (1) (2009) 132–140. doi:10.1016/j.jpowsour.2008.11.123.

[34] J. Larminie, A. Dicks, Fuel cell systems explained, second edi Edition, Wiley, 2003. doi:10.1002/9781118878330.

[35] G. Hu, J. Fan, S. Chen, Y. Liu, K. Cen, Three-dimensional numerical analysis of proton exchange membrane fuel cells (PEMFCs) with conventional and interdigitated flow fields, Journal of Power Sources 136 (1) (2004) 1–9. doi:10.1016/j.jpowsour.2004.05.010.

[36] A. Iranzo, M. Muñoz, F. Rosa, J. Pino, Numerical model for the performance prediction of a PEM fuel cell. Model results and experimental validation, International Journal of Hydrogen Energy 35 (20) (2010) 11533–11550. doi:10.1016/j.ijhydene.2010.04.129.

[37] R. Roshandel, F. Arbabi, G. K. Moghaddam, Simulation of an innovative flow-field design based on a bio inspired pattern for PEM fuel cells, Renewable Energy 41 (2012) 86–95. doi:10.1016/j.renene.2011.10.008.
URL http://dx.doi.org/10.1016/j.renene.2011.10.008

[38] W. M. Yan, S. C. Mei, C. Y. Soong, Z. S. Liu, D. Song, Experimental study on the performance of PEM fuel cells with interdigitated flow channels, Journal of Power Sources 160 (1) (2006) 116–122. doi:10.1016/j.jpowsour.2006.01.063.

[39] Ansys academic research, release 15.0, help system, fuel cell modules manuel.

[40] A. Arvay, Proton Exchange Membrane Fuel Cell Modeling and Simulation using Ansys Fluent, Masters Thesis, Arizona State University,2011.

[41] S.-H. Han, N.-H. Choi, Y.-D. Choi, Simulation and experimental analysis on the performance of PEM fuel cell by the wave-like surface design at the cathode channel, International Journal of Hydrogen Energy 39 (6) (2014) 2628–2638. doi:10.1016/j.ijhydene.2013.08.063.

II. BIO-INSPIRED FLOW FIELDS FOR PROTON EXCHANGE MEMBRANE FUEL CELLS - IDENTIFYING OPPORTUNITIES AND DEMONSTRATING APPLICATION

Joshua D. Heck, Umit O. Koylu, Ming C. Leu

Department of Mechanical & Aerospace Engineering

Missouri University of Science and Technology

Rolla, Missouri 65409–0050

Tel: 573–466–3428, Fax: 573–341–4607

Email: jdh26c@mst.edu

ABSTRACT

Bio-inspired design has emerged as a promising approach for improving the performance of Proton Exchange Membrane Fuel Cell (PEMFC) flow fields. However, in order to get the best results from bio designs, the main performance requirements of the flow field must align with those of biological flow structures. In this work the main requirement which determines the shape of biological flow structures has been identified as the need to achieve good distribution with minimal flow losses, and a design approach has been outlined for generating bio designs. To demonstrate the application of these bio design principles, a 25 cm^2 design was created, and its performance was simulated using computational modeling, along with a traditional parallel design as a reference. Furthermore, a new approach to selecting operating conditions, referred to as Water Balanced (WB) operation, is developed to help alleviate membrane dehydration or flooding issues at various points in fuel cell operation. The two designs were simulated and the bio design was shown to have 2-3 time better power output per pumping power input than the parallel design, as well as significantly better reactant distribution and product removal performance. The performance of both designs were also shown to improve when using WB operating conditions.

Keywords: polymer electrolyte membrane (PEM); fuel cell; flow distributor design; low pressure; computational fluid dynamics (CFD); bio-inspired

Highlights

- Identify the strength of bio-inspired flow fields in PEMFCs
- Develop a strategy to reduce membrane dehydration under dry reactant operation
- Demonstrate low pressure losses in bio-inspired design
- Demonstrate good reactant distribution/product removal in a bio-inspired design

Table 1. Nomenclature

Symbol	Meaning	Units
$A_{2,3}$	Cross-sectional Area of Either Main Channel in HPLR Example	cm^2
A_{act}	Active Area	cm^2
A_{HPLR}	Cross sectional Area of HPLR Section in HPLR Example	cm^2
c_p	Constant Pressure Specific Heat	$J\ kg^{-1}K^{-1}$
D_2	Diameter of Branch 2 in HPLR Example	cm
D_3	Diameter of Branch 3 in HPLR Example	cm
$D_{2,3}$	Diameter of Either Main Branch in HPLR Example	cm
D_i	Diameter of Channel i in Branching Structure	cm
D_{i+1}	Diameter of Channel $(i+1)$ in Branching Structure	cm
D_{HPLR}	Diameter of HPLR Section in HPLR Example	cm
f	Darcy Friction Factor	
F	Faraday's Constant	$C\ mol^{-1}$
I_{H_2}	Total Current Produced Based on Hydrogen Consumption	$Amperes(A)$
I_{O_2}	Total Current Produced Based on Oxygen Consumption	$Amperes(A)$
j	Current Density per Unit Area	$A\ cm^{-2}$
k	Ratio of Specific Heats	
L_2	Length of Branch 2 in HPLR Example	cm
L_3	Length of Branch 3 in HPLR Example	cm
$L_{2,3}$	Length of Either Main Branch in HPLR Example	cm
L_{HPLR}	Length of HPLR Section in HPLR Example	cm
$\dot{m}$	Mass Flow Rate of Supply Gas Mixture	$kg\ s^{-1}$
$\dot{m}_{2,3}$	Mass Flow Rate in Either Branch in HPLR Example	$kg\ s^{-1}$
$\Delta\dot{m}_{H_2}$	Mass Consumption Rate of Hydrogen	$kg\ s^{-1}$
$\Delta\dot{m}_{O_2}$	Mass Consumption Rate of Oxygen	$kg\ s^{-1}$

Continuation of Table 1		
Symbol	**Meaning**	**Units**
M_{H_2}	Molecular Weight of Hydrogen	$kg\ mol^{-1}$
M_{O_2}	Molecular Weight of Oxygen	$kg\ mol^{-1}$
$\dot{N}_{air}$	Molar Flow Rate of Dry Air	$mol\ s^{-1}$
$\dot{N}_{H_2O,gen}$	Molar Rate of Water Generation	$mol\ s^{-1}$
$\dot{N}_{tot}$	Molar Flow Rate of Humid Air Mixture	$mol\ s^{-1}$
$\dot{N}_{uptake}$	Molar Rate of Water Vapor Absorption by Cathode Supply Gas	$mol\ s^{-1}$
P_{in}	Pressure at Fuel Cell Inlet(Absolute)	Pa
P_0	Local Dead State Pressure (Absolute)	Pa
ΔP	Pressure Loss Across Fuel Cell (Gage)	Pa
$P_{sat}(T)$	Saturation Pressure of Water as a Function of Temperature	Pa
P_{mix}	Total Mixture Pressure of Humid Air	Pa
T_0	Dead State Temperature	K
$\bar{u}_{2,3}$	Average Flow Velocity in Either Branch in HPLR Example	$m\ s^{-1}$
$\dot{W}_c$	Compressor Power to Pump Supply Gas	W
$\dot{W}_{fc}$	Power Output of Fuel Cell Unit	W
$X_{H_2O,in}$	Mole Fraction of Water Vapor at Inlet	
$X_{H_2O,out}$	Mole Fraction of Water Vapor at Outlet	
$X_{H_2O,max}$	Maximum Mole Fraction of Water Vapor at Specified T and P	
Greek Symbols		
η_c	Compressor Efficiency	
ρ	Supply Gas Density	$kg\ m^{-3}$
ξ	Stoichiometry (Ratio of Reactant Supply to Amount Consumed)	
End of Table		

1. INTRODUCTION

Proton Exchange Membrane Fuel Cells (PEMFCs) have emerged as a promising candidate for power generation due to their clean local operation, good operating efficiency, quiet opperation, and short startup time, among other things [1]. The only local product of PEMFC operation is water and, if clean methods are used to produce hydrogen, PEMFCs can have net-zero-emission power production [2]. Additionally, since PEMFCs are a direct energy conversion device, higher operating efficiencies can be realized than those attainable by conventional energy conversion methods that rely on the intermediate heat step [3]. Despite these advantages, PEMFCs have not yet achieved the durability and reliability required in order to successfully replace established methods. One of the key elements of durability and reliability of PEMFCs is the ability to achieve good distribution of reactants and effective removal of products over the active area of the catalyst. Maldistribution of reactants and ineffective product removal lead to uneven chemical reaction rates over the catalyst area, hot spots, and large water concentration gradients that negatively impact the mechanical and chemical integrity of the polymer membrane [4, 5]. Additionally, fuel cell performance is sensitive to operating conditions such as temperature, reactant concentration, and relative humidity [6]. While the operating conditions may be nominally set by controlling the state of the supply gases, the local distribution over a fuel cell active area is highly dependent on the geometry of the flow fields in the bi-polar plates. For this reason, flow field design has been the subject of many past works [7, 8] and is still an active area of research.

One promising design strategy which has emerged for improving the performance of flow fields is the idea of using biologically-inspired (bio) designs which mimic the geometry of naturally occurring vascular structures. Several bio designs have been proposed in prior literature. Tuber et al. [9] developed a methodology whereby a “multiple-branched structure with ‘smooth’ flow paths similar to biological fluid channels" could be generated for an arbitrary active area. They then tested designs in both PEM and direct methanol fuel cells

(DMFCs), comparing their performances to those of the traditional parallel and serpentine designs. Kloess et al. [10] tested two designs, both interdigitated style, which they called leaf and lung designs, and compared their performances to those of the traditional single serpentine and interdigitated designs. Wang et al. [11] reported an initial bio-design with a series of dividing and combining channels, and two more iterations on the design, all of which are parallel style, in follow-up work [12]. The parallel and single serpentine designs were used a references for performance comparison. Currie [13] applied biomimetic design principles to make several alterations to the traditional parallel design, as well as creating three new biomimetic designs, and compared their performances to those of the parallel and multi serpentine designs. Roshandel et al. [14] presented a parallel style bio design based on a leaf that used a parallel type configuration, and tested three different branch angles, 30, 45, and 60 degrees, and compared the performance to the parallel and single serpentine designs.

Guo et al. [15] presented three variations on a bio design based on a leaf pattern, one with constant width branches and parallel configuration, one with constant width branches and interdigitated style, and one with varied width branches and interdigitated style. All of these desings were compared to the traditional interdigitated and parallel-in-series (also called multi-serpentine) designs. Further work was performed on characterizing the water transport properties of these bio designs by Saripella et al. [16], using only the single serpentine design for comparison.

Arvay et al. [17] proposed multiple biologically inspired flow field designs of both parallel and interdigitated style, and compared with the parallel, single serpentine and interdigitated traditional designs. Ozden et al. [18] recently investigated the application of biologically inspired designs in DMFCs. The performance of a DMFC using the "Lung Design" of Kloess [10] as well as two new designs were presented and compared to that of the multi-serpentine design.

In these previous works, varying levels of explanation were provided as to what aspects of the proposed designs were inspired by biological flow structures, and emphasis has been given mainly to how to mimic the geometry of biological flow structures. However, no concerted effort has been made to identify what the main defining characteristics of biological flow structures are, what the specific strengths and purposes of those structures are, and how they can best be applied to the design of fuel cell flow fields. In order for the application of bio-design to be beneficial to fuel cells, flow field performance goals must align with the purpose of biological flow structures. Fuel cells operate in a broad range of applications, requiring an equally broad range of system constraints and operating regimes, and not all of them will align well with the motivations which shape biological flow structures. In this work, the key characteristics and strengths of biological flow structures will be identified, and fuel cell operating modes will be considered to find the analogous operating regime which matches the performance goals of biological flow structures. A design strategy whereby bio designs can be generated to take full advantage of the natural strengths of biological flow structures will then be developed. Furthermore, a new method of selecting operating conditions is developed which helps to alleviate water management issues. Finally, in order to demonstrate the design principles and operating mode, an example PEMFC bio design is presented and the performance is simulated computationally using two sets of operating conditions, along with the traditional parallel design for comparison.

2. IDENTIFYING STRENGTHS OF BIO-INSPIRED DESIGN

2.1. Characteristics of Biological Flow Structures. Several preceding authors [13, 15–18] have utilized a principle of physiology called “Murray’s Law", which is a relationship for the relative size of successive branches in biological flow systems. Sherman [19] gave an explanation and derivation of this law, which Murray simply called “The Physiological Principle of Minimum Work" [20] applied to channel diameters. This law states that, when a parent branch (generation i) splits into n daughter branches (generation

$i + 1$), the sum of the cube of the diameters of all daughter generation channels (D_{i+1}) is equal to the cube of the diameter of the parent channel (D_i),

$$D_i^3 = \sum D_{i+1}^3. \tag{1}$$

The D^3 relation, which has come to be known as Murray's Law, comes from the physiological principle of minimum work applied to branch diameters, but there is actually more than one application of this principle. Murray also applied it to branching angles and flow path lengths [21]. The basis of this principle is as follows.

While the purpose of the vascular system in an organism is to transport necessary reactants and remove waste products from metabolic activity, an organism must turn some of its metabolic energy into flow energy to facilitate vascular circulation. It is undesirable for the organism to use a large amount of metabolic energy in the process. Thus, since larger flow carriers would reduce the viscous dissipation of flow energy (pressure loss), there is a driving motivation for larger vessels. However, since the vascular material in biological flow structures is living tissue, it also uses metabolic energy, and increasing the size of the flow carriers means that more metabolic energy will be consumed by the vascular tissue. So there is a limit to which increasing the size of the vasculature, and thereby reducing flow losses, actually benefits the organism. As a final constraint, the vascular system should supply every region of the organism in the appropriate proportion. Under-supplied tissue would die from lack of nutrients, and over supply of any region would simply be a waste of metabolic energy by pumping more fluid than was required. Murray [20, 21] showed that the geometry of biological flow structures, both in the channel diameter, and in path lenghts and branching angles, is optimized to balance these competing requirements. The result is large parent channels which carry bulk flow from a central location and then strategically branch into smaller generations near the target area following the D^3 law for optimal distribution with minimal flow losses. Thus, *the geometry of biological flow structures is optimized to*

effectively distribute reactants and remove products with minimal flow losses. In order for the application of bio-design to be most beneficial to fuel cell flow field performance, the design motivation for the flow field must align with this goal.

2.2. Analogous Fuel Cell Operating Regime. There is a wide range of applications to which PEMFCs are well suited and many of these various applications call for different system designs and operating regimes. The analogous operating mode in a fuel cell system is the case in which it is desirable to operate with minimal auxiliary system power and complexity. Reducing the auxiliary system requirements involves both reducing the pumping power requirement, which is directly impacted by the pressure drop across the flow field, and reducing any power or equipment associated with humidification, which may require the fuel cell to operate with low humidity or "dry" reactants. Additionally, the same requirement to distribute reactant to every portion of a fuel cell's active area exists, as any stagnant area quickly runs out of reactant, and can be considered a "dead spot" in the fuel cell, as the catalyst is not being utilized. This means that both low pressure loss and good distribution would be of primary concern, as in biological flow systems. Since the ribs between channels on the bipolar plate are responsible for current collection from the GDL, there is a requirement that channels may not be arbitrarily large, as mass distribution of reactant must be balanced with current collection needs, similar to the limitations on biological vessel size due to metabolic energy utilization of vascular tissue. The condition of maintaining a balance between channel area and rib/GDL contact area is present in all fuel cell applications. Thus, *the particular strength which bio design has to offer is providing good reactant distribution in the channels when low pressure drop is a dominant requirement.*

2.3. Effect of Interdigitation. An important consideration in flow field design is that the geometry will influence the mass transport mechanism by which reactants are transported from the channel layer across the Gas Diffusion Layer (GDL) to the catalyst layer. Mass transport of the reactant species from channel to catalyst layer occurs through

diffusion due to the concentration gradient created by consumption of reactants at the catalyst layer. However, bulk convective flow can also be driven through the GDL sufficient pressure gradients are present. The geometry of the flow field will determine which of these mechanisms is dominant. These effects may be observed in three of the most well documented traditional designs, the parallel, interdigitated, and single serpentine designs. The parallel design is dominated everywhere by diffusion since no appreciable pressure difference is developed between adjacent channels, such that there is no driving potential for convective flow through the GDL. The interdigitated design, introduced by Nguyen [22], intentionally has two discontinuous sets of channels; once set connected to the inlet and the other connected to the outlet, which are arranged so that each inlet channel is adjacent to an outlet channel. In this way, the only path that the flow can take from inlet to outlet is to pass through the GDL, and this design is dominated by convective flow. The single serpentine consists of a single channel which passes back and forth across the active area by making a series of 180° bends. Feser et al. [23] showed that, due to the major and minor pressure losses in the long stretches of channels and 180° bends, significant pressure differences can develop between adjacent channels far from a bend, which induces local convective flow, while near the bends the mass transport of reactant is still predominately diffusive. (In this work the terms "parallel style" and "interdigitated style" will be used to designate designs which are continuous from inlet to outlet and rely predominately on diffusive transport, and designs which have discontinuous channels and rely mainly on convective transport, respectively.)

Whether to use a parallel or interdigitated style geometry is a decision which must be made early on in the design process when creating a new flow field geometry. Among previous works on bio-inspired designs there has been a mix of both parallel and interdigitated style designs proposed. The enhancement of mass distribution provided by inducing convective flow in the GDL makes interdigitation an attractive design feature in many applications. However, in consideration of the primary application area of bio design, namely

providing good distribution with minimal pressure losses, there are two reasons why an interdigitated style should not be used: 1) a large pressure gradient is required to force convective flow through the GDL, and 2) the large pressure loss incurred in under rib flow dominates the distribution characteristic of the flow field, making the channel geometry of little impact on fuel cell performance.

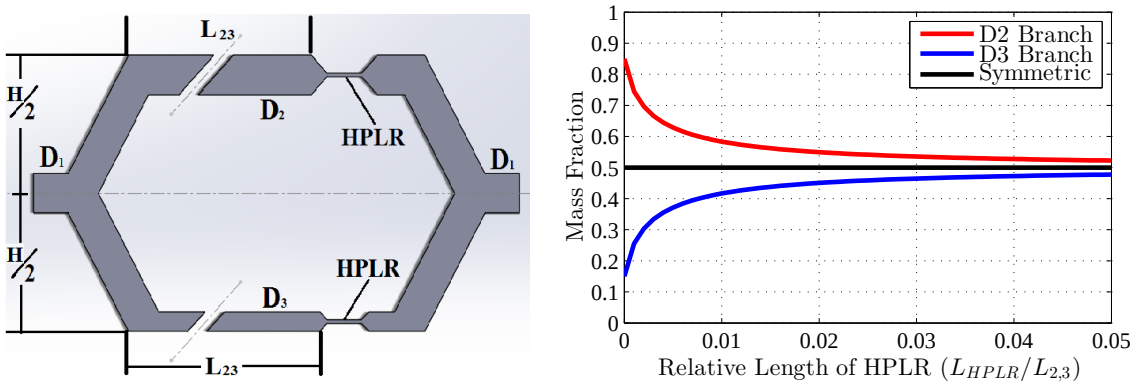

(a) Diagram of HPLR in parallel flow paths

(b) Plot of the effects of the HPLR of flow distribution

Figure 1. Effect of HPLR on flow distribution- (a) diagram of simplest parallel flow case, and (b) effects of HPLR on flow distribution

A fuel cell flow field is simply a network of parallel flow paths. As an example of the effect of interdigitation on flow distribution, the simplest parallel flow network having only two flow paths may be considered. Shown in Figure 1 (a) is a two path parallel flow network of equal length flow paths in which the diameter of one path, D_2, is twice that of the other, D_3, but both have an identical section of reduced diameter which is labeled as a High Pressure Loss Restriction (HPLR). Using the standard internal flow modeling method of friction head loss analysis [24], the mass flow rate through each of these branches may be determined. Ignoring minor loses, the total pressure drop, ΔP, across either of the possible

flow paths would be

$$\Delta P = \rho \frac{\bar{u}_{2,3}^2}{2} \left(f \frac{L_{2,3}}{D_{2,3}} + \left(\frac{A_{2,3}}{A_{HPLR}} \right)^2 f \frac{L_{HPLR}}{D_{HPLR}} \right) \tag{2}$$

where ρ is the density, $\bar{u}_{2,3}$ is the average velocity in the channel under consideration (either 2 or 3, as labeled in Figure 1 (a)), f is the Darcy Friction Factor, $L_{2,3}$ is the length of the main channel section, $D_{2,3}$ is the diameter of the main channel section, $A_{2,3}$ and A_{HPLR} are the cross sectional areas of the main branch under consideration and the HPLR section, and L_{HPLR} and D_{HPLR} are the length and diameter of the HPLR section, which are identical for either flow path. Note that the area ratio $A_{2,3}/A_{HPLR}$ comes from applying the continuity equation to get a relationship between the velocity in the HPLR section to that in the main channel section so that only the velocity head in the main channel ($\rho \bar{u}_{2,3}^2/2$) need be used. Equation 2 may then be rearranged to find the mass flow through each branch as

$$\dot{m}_{main} = A_{2,3} \sqrt{\frac{2\rho\Delta P}{f \frac{L_{2,3}}{D_{2,3}} + \left(\frac{A_{2,3}}{A_{HPLR}} \right)^2 f \frac{L_{HPLR}}{D_{HPLR}}}}. \tag{3}$$

These equations have been implemented for the configuration shown in Figure 1 (a) with main flow channel diameters with $D_2 = 2 \times D_3$, a length of $L_{2,3} = 10 \times D_2$, and an HPLR section diameter of $D_{HPLR} = (1/5) \times D_2$. Equation 3 was applied while allowing the length of the HPLR section to vary from $0 \times L_{2,3}$ (no restriction case) to $(1/20) \times L_{2,3}$, and the resulting mass distributions are shown in Figure 1 (b). The solid black line at a constant mass fraction of 50% is the case where the two branches are symmetric in length and diameter ($D_2 = D_3$ and $L_2 = L_3$) in which uniform distribution is achieved. For the red and blue lines ($D_2 \neq D_3$ and $L_2 = L_3$ case) to the far left on this graph is the case of no HPLR section, in which the different channel diameters result in a mass flow split of 85% passing through the larger D_2 channel and only 15% passing through the smaller D_3 channel. The addition of an HPLR section very quickly begins to drive the mass fractions back towards

a uniform distribution, however at the cost of requiring a much higher pressure differential to drive the same amount of flow. Compared to the unrestricted case, approximately two orders of magnitude more pressure is required to drive the same amount of flow through these parallel flow channels with a $(1/20) \times L_{2,3}$ HPLR section.

The same phenomenon appears in fuel cell flow field designs which make use of Interdigitation. The major and minor pressure losses in the channels are typically on the order of 10^2 Pascals in the traditional interdigitated design configuration, which is very similar to the traditional parallel design. However, in order to drive the under-rib convective flow through the porous GDL material a pressure loss on the order of 10^4 Pascals is often encountered. The vast majority of the pressure loss occurs as the flow is forced through the GDL, and this high pressure loss compared to that of the channel flow functions in the same way as the previously demonstrated HPLR case. The HPLR effect of under-rib flow tends to drive the flow pattern in the channels towards a uniform distribution, and dominates the effect of channel geometry on the flow distribution characteristics of interdigitated designs. This effect on distribution along with the performance enhancement due to the increased mass transport capabilities of convective flow in the GDL can be of great advantage to fuel cell designers who do not have to be concerned with minimizing the pressure losses across the flow field. The combined effects can yield gains in fuel cell power output that outweigh the losses incurred in increased pumping power required. However, the high pressure losses incurred, and the domination of flow distribution by the HPLR effect over that of the channel geometry effectively negate all advantages of using bio design.

2.4. Design Methodology for Creating Bio-Inspired Flow Fields. Based on the principles highlighted in the preceding section and some further observations on biological flow structures, a set of design principles was developed for creating bio-inspired flow field geometries. To distribute reactants from a central location over a large area, biological flow systems use networks of branching channels, a feature which should be mimicked in flow field design. Biological systems are often symmetrical, a feature which may be used to

control the distribution of flow in fuel cells, so symmetry should be taken advantage of as often as possible. Channel sizes are not uniform in biological flow structures, but rather the size of a channel is proportional to the amount of reactant that must be transported. This is the fundamental basis of Murray's D^3 law. Murray's Law for channel size has been applied directly in this work, under two constraints. Since the channels in a fuel cell should not be too small or too large in order to balance mass transport and current collection needs, Murray's Law was applied within lower and upper limits on channels sizes of 1 mm and 3 mm, respectively. (The ribs are of constant 1 mm width.) Murray's relations for branching angles was developed to minimize the flow losses for the case of "free unobstructed branching of vessels" [21], and the optimum angle of branches depend on their relative diameters. Since the channels in a fuel cell flow field are required to be closely spaced with ribs between them to balance mass transport and current collection needs, this is not a case of free unobstructed branching, and Murray's Law for Branching Angles was not applied directly. However, for branches which are of similar sizes, biological systems tend to avoid both large (near 90°) and small (near 0°) branching angles, opting rather for intermediate values near the middle of this range. In this work, a constant branching angle of 45° was used. In the same vein of thought, biological systems rarely form square or rectangular geometries, and the designer should not be constrained to such geometries. Right angle corners can form stagnation points in parallel network type flow systems such as fuel cell flow fields. In this work, the shape of the active area has been altered from the traditional rectangular geometry to eliminate this issue. The total aspect ratio of the minimum rectangular envelope which would enclose the bio design is 2x1, and the rectangular parallel design, which is used as the reference case, has the same aspect ratio. The flow field designer should avoid creating preferential flow paths, such as the case of a set of large parent channels traveling directly from inlet to outlet, having only

a very short section of daughter channels connecting them. Lastly, as has been shown in Section 2.3, using interdigitation effectively eliminates all advantages of bio design, and so interdigitation should be avoided. These design principles are summarized here:

1. Use branching geometry
2. Take advantage of symmetry when possible
3. Channel should be sized proportionally to their volume flow requirements (D^3 law)
4. Branching angles should not be extreme (avoid 90 degree bends)
5. Do not constrain the flow field geometry to the traditional rectangular area
6. Avoid preferential flow paths- Match resistance with available potential
7. Avoid interdigitation

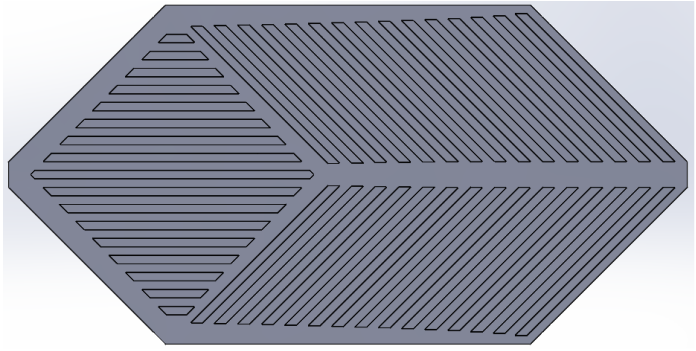

(a) Bio-inspired design

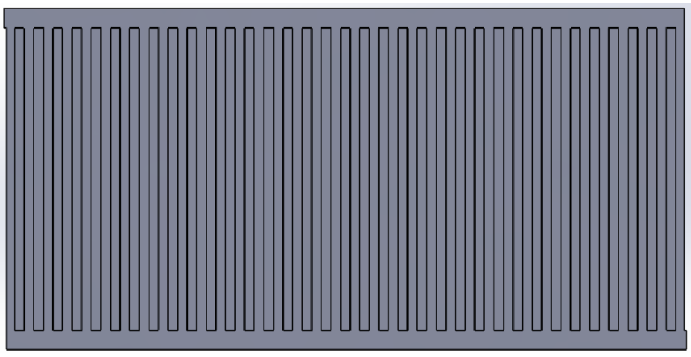

(b) Parallel 2x1 aspect ratio

Figure 2. Flow field designs (a) bio-inspired design created for demonstration (inlet at left, outlet at right) (b) parallel 2x1 aspect ratio for comparison (inlet top left, outlet bottom right)

As an example, these principles were used to create a 25 cm^2 design, which is shown in Figure 2 (a). Using numerical simulations the performance of this design was compared to that of a traditional parallel design, shown in Figure 2 (b), and the details of these geometries are given in Table 2.

Table 2. Flow field geometry parameters for parallel and bio designs

Geometric Parameter	**Value**	**Units**
Parallel Design		
Active Area	25	cm^2
Length	70.7	*mm*
Width	35.4	*mm*
Number of Channels	36	
Channel Branch Angle	90	°
Channel Area Ratio	56.1	%
Channel Depth	1.5	*mm*
Channel Width	1.0	*mm*
Rib Width	1.0	*mm*
Bio Design		
Active Area	25	cm^2
Length (inlet to outlet)	79.8	*mm*
Width	26.1	*mm*
Number of Minimum Diameter Channels	46	
Channel Branch Angle	45	°
Channel Area Ratio	60.2	%
Channel Depth	1.5	*mm*
Channel Width (Minimum)	1.0	*mm*
Channel Width (Maximum)	3.0	*mm*
Rib Width	1.0	*mm*

The design shown in Figure 2 (a) is only one possible configuration resulting in the application of these principles, and is in no way optimized. Undoubtedly this design could be improved by using variable sizes on the final generation of channels, optimizing the branching angles for this configuration, changing the upper and lower constraints on the channel dimensions, or optimizing with respect to any other geometric parameter of the flow field. Such topics are beyond the scope of this work. The purpose of the example

geometry is to demonstrate that, even without optimization, through the application of these design principles, flow fields may be created with better distribution performance at lower pressure drop than the best conventional low-pressure drop design has to offer.

3. OPERATING CONDITIONS

When choosing operating conditions at which to test the performance of bio flow fields, the operating conditions should align with the design constraint of minimizing auxiliary system requirements. In this work, untreated atmospheric air was used for the cathode supply gas in order to eliminate any heating or humidification system for the cathode. Since both heat and water are produced at the fuel cell cathode, the cathode gas can be heated and humidified by normal fuel cell operation. The total auxiliary system for processing cathode supply gas is then reduced to a single pump. By using a passive membrane humidifier, the anode supply gas may be heated and humidified by the cathode exhaust gas. In addition to hydrogen storage at high pressure, only a single passive membrane humidifier which recovers product water and waste heat from the cathode exhaust, and, optionally, an anode re-circulation pump is required. The sizes and power requirements of the pumps will be dependent on the pressure loss of the flow field, so minimal pressure losses, provided by the bio flow fields, are critical in minimizing the auxiliary system.

The nominal operating temperature and pressure of the fuel cells were 50 °C and 1 atm for all cases. The relatively low operating temperature reduces auxiliary heating and humidification requirements. Note that while these two designs were allowed to exhaust to atmospheric pressure, they have very low pressure drops, as the maximum variation at the inlet from atmospheric pressure was only 0.1%, so the pressure was taken to be 1 atm for the purpose of calculating inlet conditions. Two operating modes were simulated to demonstrate the designs' reactant distribution and water removal characteristics: 1) constant flow rate and 2) Water Balanced (WB) constant stoichiometry which will be explained later in detail. For both cases the cathode inlet conditions were selected to represent un-treated ambient

air, and the anode inlet conditions were fully humidified hydrogen at the fuel cell operating temperature and pressure. For the constant mass flow rate case, the mass flow rates were set such that at a current density of 1.0 $A\ cm^{-2}$, the anode and cathode stoichiometries would be 1.2 and 2.0, respectively. This means that relatively high stoichiometries are encountered when operating at lower current densities.

Water management is always a concern in PEMFCs. When operating with fully humidified reactants, membrane drying is unlikely while the main concern is removing excess product water at high current densities. In most cases, when operating with fully humidified reactants, cell performance increases monotonically with increasing mass flow rate. However, when operating with dry cathode supply gas, membrane dehydration can be a serious concern if the mass flow rate is too high [25, 26], while enough water may still be produced at high current densities to cause mass transport limitations with low mass flow rates. Thus, the issue of water management is doubly important when operating with dry supply gas.

In order to alleviate this issue, a new operating strategy was devised. Using untreated atmospheric air in the cathode, the air enters at low temperature with some small initial water vapor content, and exits the fuel cell at some higher temperature, and carrying some additional water content, produced from the electrochemical reactions. The maximum mole fraction of water vapor which can be contained in a humid air mixture, $X_{H_2O,max}$, is a function of both mixture temperature and pressure and, from the definition of relative humidity, the relationship is given by

$$X_{H_2O,max} = \frac{P_{sat}(T)}{P_{mix}}, \tag{4}$$

where $P_{sat}(T)$ is the saturation pressure of water as a function of temperature, and P_{mix} is the total mixture pressure. Figure 3 shows the variation of the maximum mole fraction of water vapor in fully saturated air (100 % relative humidity) with temperature and pressure by applying Equation 4 over the range of 0-100 °C for several fixed mixture pressures.

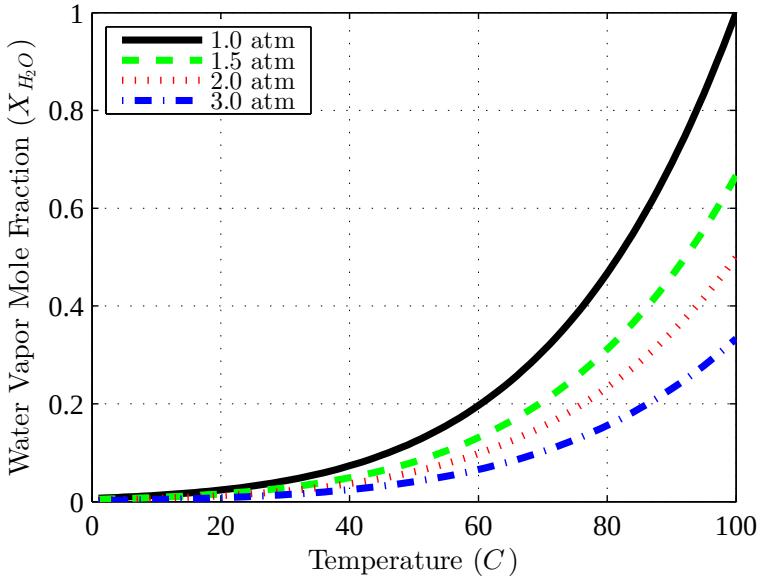

Figure 3. Variation of water vapor mole fraction at 100 % relative humidity with temperature and pressure

Note that with an increase in temperature or a decrease in pressure, the capacity of air to hold water vapor increases. Li et al. [27] took advantage of this fact and devised a design strategy to match the water uptake capability of the cathode to the water production rate in the fuel cell. The dimensions and number of channels in a multi-serpentine configuration were selected to induce a specific pressure drop across the flow field, such that with a known temperature difference between inlet and outlet, the outlet relative humidity would be 100%. This is possible in a serpentine configuration fuel cell as the pressure loss across the flow field is significant. However, this strategy cannot be directly applied to low pressure drop flow fields, such as bio designs.

A similar strategy was devised that utilized the temperature difference between inlet and outlet directly when operating with dry air, rather than relying on a large pressure drop. Cathode air was supplied at low temperature and, assuming that the cathode exhaust exits at or near the nominal operating temperature, the mass flow rate could be selected such that the outlet relative humidity was 100%.

The molar rate at which water is produced from the electrochemical reactions, $\dot{N}_{H_2O}$, in the fuel cell cathode is

$$\dot{N}_{H_2O,gen} = \frac{jA_{act}}{2F}, \tag{5}$$

where j is the current density, A is the active area, and F is Faraday's constant. The rate at which the cathode air can absorb additional water vapor, $\dot{N}_{uptake}$, due to the temperature rise between inlet and outlet is given by

$$\dot{N}_{uptake} = \left(\frac{X_{H_2O,out}}{1 - X_{H_2O,out}} - \frac{X_{H_2O,in}}{1 - X_{H_2O,in}}, \right) \dot{N}_{air} \tag{6}$$

where $X_{H_2O,in}$ and $X_{H_2O,out}$ are the mole fractions of water vapor at the inlet and outlet, respectively, and $\dot{N}_{air}$ is the mass flow rate of dry air.

Knowing the inlet conditions and assuming the temperature at the outlet is approximately equal to the nominal operating temperature, the required mole fraction of water vapor to attain 100% relative humidity may be calculated. Then, by setting the rate at which water is produced by the electrochemical reactions ($\dot{N}_{h_2O,gen}$) equal to the uptake rate ($\dot{N}_{uptake}$), the flow rate of dry air ($\dot{N}_{air}$) which will result in an outlet relative humidity of 100 % may be calculated from Equations 5 and 6 as

$$\dot{N}_{air} = \frac{\frac{jA}{2F}}{\frac{X_{H_2O,out}}{1-X_{H_2O,out}} - \frac{X_{H_2O,in}}{1-X_{H_2O,in}}}, \tag{7}$$

and the total mixture molar flow rate at the inlet is then given by

$$\dot{N}_{tot} = \left(\frac{1}{1 - X_{H_2O,in}}\right)\dot{N}_{air}. \tag{8}$$

Since there is a fixed ratio between the current density and the total flow rate, this means operating at a fixed stoichiometry. Presuming the mole fraction of oxygen in dry air to be 0.21, the stoichiometry at which Water Balanced (WB) operation can be achieved is

$$\xi = \frac{0.42}{\frac{X_{H_2O,out}}{1-X_{H_2O,out}} - \frac{X_{H_2O,in}}{1-X_{H_2O,in}}}. \tag{9}$$

This method was used to determine the cathode stoichiometry, while the anode was set at a stoichiometry of 1.5. Using an inlet temperature of 25 °C, inlet relative humidity of 50%, and presuming an outlet temperature of 50 °C and target relative humidity of 100%, the required cathode stoichiometry to achieve WB operation was determined to be 3.5. The operating conditions used for both the fixed mass flow rate, and water balanced fixed stoichiometry cases are given in Table 3, and the mass flow rates for both anode and cathode in the fixed stoichiometry case are given in Table 4.

It should be noted that the method of determining water balanced operating conditions may only be used at relatively low outlet temperatures. In the limiting case, with the minimum possible operating stoichiometry of 1.0, the fuel cell will produce enough water to achieve 100 % relative humidity for an outlet temperature of approximately 70 °C, so this is the upper limit of operating temperature for which this method can be used. However, since low temperature operation fits well with the constraint of minimizing the auxiliary system, these operating conditions are well suited for bio design applications.

Table 3. Inlet conditions

Inlet Property	Value	Units
Common Parameters		
Anode Temperature	50	°C
Anode Pressure	1	atm
Anode Humidity	100	%
Anode Water Mole Fraction	0.120	
Anode Hydrogen Mole Fraction	0.880	
Cathode Temperature	25	°C
Cathode Pressure	1	atm
Cathode Humidity	50	%
Cathode Water Mole Fraction	0.016	
Cathode Oxygen Mole Fraction	0.207	
Cathode Nitrogen Mole Fraction	0.778	
Fixed Mass Flow Case		
Anode Mass Flow Rate	6.96×10^{-7}	$kg\ s^{-1}$
Cathode Mass Flow Rate	1.80×10^{-5}	$kg\ s^{-1}$
Fixed Stoichiometry Case		
Anode Stoichiometry	1.5	
Cathode Stoichiometry	3.5	

Table 4. Mass flow rates for water balanced operation

$j(Acm^{-2})$	$\dot{m}_{an}\ (kgs^{-1})$	$\dot{m}_{ca}\ (kgs^{-1})$
0.1	8.70×10^{-8}	3.15×10^{-6}
0.2	1.74×10^{-7}	6.29×10^{-6}
0.3	2.61×10^{-7}	9.44×10^{-6}
0.4	3.48×10^{-7}	1.26×10^{-5}
0.5	4.35×10^{-7}	1.57×10^{-5}
0.6	5.22×10^{-7}	1.89×10^{-5}
0.7	6.09×10^{-7}	2.20×10^{-5}
0.8	6.96×10^{-7}	2.52×10^{-5}

4. COMPUTATIONAL METHODS

4.1. Mesh and Model Parameters. The commercial software package ANSYS Fluent 15.0 was used to perform a computational study on the performance of the bio and parallel flow field designs presented in Section 2.4 using the PEMFC Add-On Module. The present authors have experimentally validated CFD results for various flow field designs

in previous work [15, 16] using the same software package, and the computational study performed for the present work was based on the same model parameters, as well as the work of Iranzo et al. [28].

Table 5. Fuel cell geometry and material properties

Component	**Value**	**Units**
BPP Thickness	2.50	mm
BPP Electrical Conductivity [28]	926	$S\ cm^{-1}$
GDL Thickness	0.35	mm
GDL Porosity	0.80	
GLD Electrical Condictivity [28]	2.80	$S\ cm^{-1}$
Catalyst Thickness	0.01	mm
Catalyst Porosity	0.80	
Membrane Thickness	0.15	mm
Membrane Equivalent Weight [28]	1100	$kg\ kmol^{-1}$

The flow field geometries were given in Table 2 in Section 2.4, and the layer thicknesses and select material properties are provided in Table 5. Both designs were meshed with the ANSYS Workbench 15.0 Meshing application. A mesh study was performed on both quality and number of elements to ensure stable convergence and mesh independence. The final mesh used for the parallel design contained 1.616 million hexahedral elements with a minimum orthogonal quality of 0.966, and the bio design contained 1.912 million elements of hexahedral and wedge type to accommodate the angled branches, with a minimum orthogonal quality of 0.625. The maximum mesh size was set to 0.25 mm, which was the maximum spacing in the in-plane direction for all layers. The spacing in the through-plane direction was varied as necessary in order to fit cells within the thinner layers. The channel layer had 6 cells across, and all other layers were 4 cells across, as can be seen in Figure 4.

In addition to mass, momentum, energy, and species conservation equations that are routinely solved in CFD modeling, additional models are required for fuel cells computations. Joule and reaction heating, electrochemistry sources for the species model,

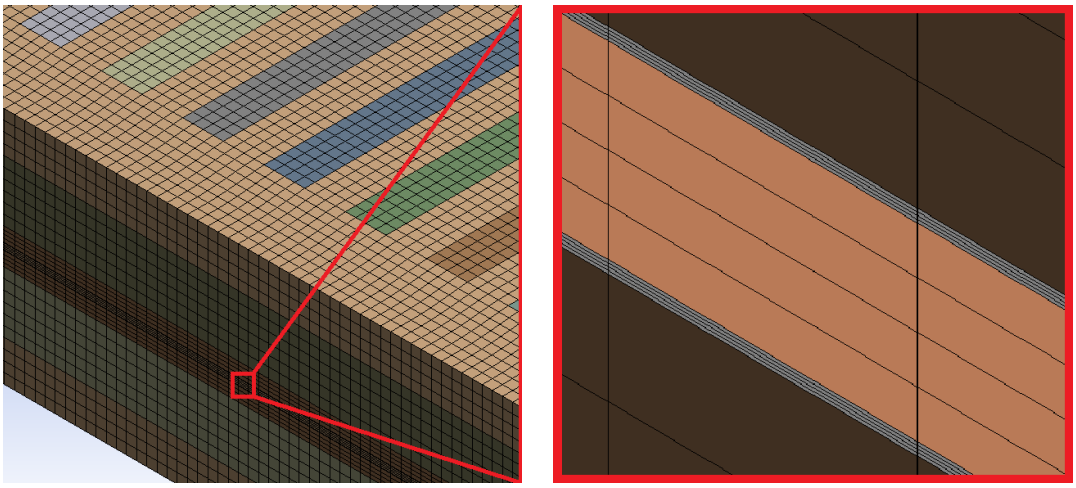

(a) Mesh- layers and channel view (b) Detail of catalyst and electrolyte Layers

Figure 4. Mesh- (a) cut view of all through plane mesh layers and (b) detail of catalyst and electrolyte layers (color cersion available online)

Butler-Volmer reaction rate, and multiphase models, along with electrical potential and electronic and protonic conduction are also solved to simulate fuel cell performance. It should be noted that two phase flow for condensed water vapor is not fully simulated, but rather the assumption is made that any condensed water travels with the free stream velocity in the channel layer as a fine mist. The effect of blockage by liquid water in the porous zones (GDL and Electrolyte) is approximated by multiplying porosity by $(1 - s)$, where s is the volume fraction of liquid water. Additional model details can be found in [29].

The SIMPLE (Semi-Implicit Method with Pressure Linked Equations) solver was used, with least squares cell based gradient, while the discretization set to standard for pressure and second-order upwind for all other parameters. A constant temperature boundary condition of 323 K was used for all exterior walls. Inlet boundary conditions for temperature and species were previously given in Table 3, Section 3, and a constant pressure boundary condition of 1 atm was used at all outlets. Table 6 lists the parameters specific to fuel cell modeling used in the present study.

Table 6. Numerical model parameters used in the fluent simulations

Model Parameter	**Units**	**Values**
Ref. Current Density- Anode	A/m^3	4.48×10^5 [15]
Ref. Current Density- Cathode	A/m^3	4.48 [15]
Catalyst Layer Surface to Volume Ratio	m^{-1}	1.25×10^7 [15]
Ref. Concentration- Anode	$kmol/m^3$	1.0
Ref. Concentration- Cathode	$kmol/m^3$	1.0
Concentration Exponent- Anode		0.5 [28]
Concentration Exponent- Cathode		1.0 [28]
Exchange Coefficient- Anode		1.0 [15]
Exchange Coefficient- Cathode		1.0 [15]
Open Circuit Voltage	$Volt$	1.0
Leakage Current	A	0.0
Reference Diffusivity- H_2	m^2/s	8×10^{-5} [15]
Reference Diffusivity- O_2	m^2/s	2×10^{-5} [15]
Reference Diffusivity- H_2O	m^2/s	5×10^{-5} [15]
Saturation Exponent (Pore Blockage)		2.0 [28]

4.2. Simulation Strategy and Convergence Criteria. For the constant mass flow rate cases, potentiostatic boundary conditions were used with voltage points being run from 0.25 to 0.85 volts in 0.1 volt increments, with an open circuit voltage of 1.0 volts. It was found that the rate of convergence was greater with potentiostatic boundary conditions, so for the fixed mass flow rate case, they were used to in order to reduce computational time. For simulating fixed stoichiometry operation for the water balanced cases, galvanostatic boundary conditions must be used, and the computations were run at 0.1 A/cm^2 increments up to 0.8 A/cm^2. In both cases, the first point run was started from a default initialization, and when convergence for that point was reached and the data file saved, the voltage or current destiny for the respective cases was adjusted to the next set point and the simulation continued to solve for the next operating point. This process of starting from the converged solution of the preceding point was used for all remaining points.

In determining when the solution for each set point was considered to have converged, it was necessary to look further than the standard method of residuals reduction when using the PEMFC Module. It was found that species and current conservation would

not be satisfied until several thousand iterations after apparent convergence was achieved based solely on the residuals, as previously noted by Arvat et al. [30]. Naturally, in order to gain insights to the details of flow field performance, current and species model convergence must be attained. It was found that the coupled current and species models were the slowest to converge, and therefore total current and species values were monitored directly in order to ensure convergence.

The total current at the terminals and mid-plane of the fuel cell (Cathode, Anode, and Electrolyte Currents), as well as the rate of hydrogen and oxygen consumption due to electrochemical reactions ($\Delta\dot{m}_{H_2}$ and $\Delta\dot{m}_{O_2}$) were monitored. In order to ensure that not only the current at all planes in the fuel cell are in agreement but also the species model, which is coupled by electrochemistry source terms, are all in agreement, the consumption rates of oxygen and hydrogen may be used to calculate an equivalent current. The current produced by the electrochemical reactions of hydrogen and oxygen may be determined by

$$I_{O_2} = \frac{4F}{M_{O_2}}\Delta\dot{m}_{O_2}, \tag{10}$$

$$I_{H_2} = \frac{2F}{M_{H_2}}\Delta\dot{m}_{H_2}. \tag{11}$$

When the current values at each plane in the fuel cell along with the predicted current values from the consumption rates of hydrogen and oxygen all agreed to within 1%, the solution was considered to have converged. Figure 5 shows a representative convergence plot where the predicted total current and species currents are plotted against iteration count.

If the simulation is stopped prematurely based on monitoring residuals only, apparent results may be obtained, but they would not be reliable as the currents at different planes in the fuel cell would not agree. Additionally, the species data, which is of particular interest for this work, is the last to converge, as can be seen in Figure 5. Even monitoring the current

data directly would not be enough because the hydrogen data would still not satisfy the coupled mass conservation and electrochemistry models. Thus, it is imperative to monitor all of the quantities associated with the electrochemistry models for convergence criteria.

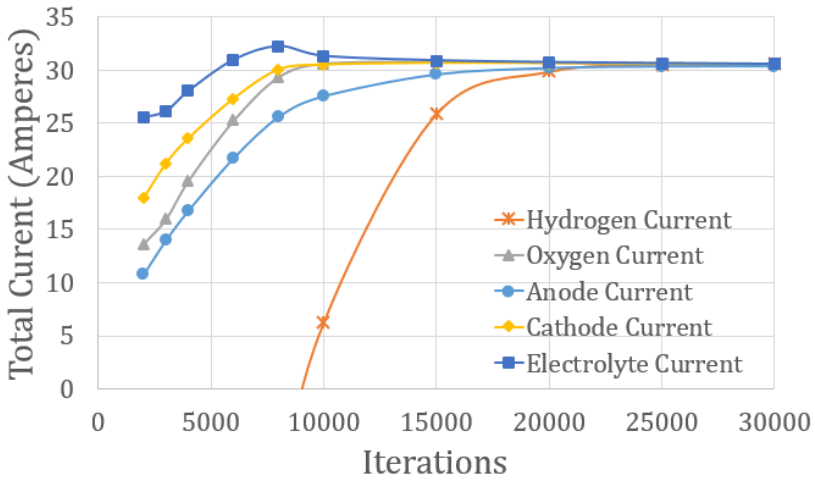

Figure 5. Example convergence plot demonstrating species and current tracking

5. PERFORMANCE OF EXAMPLE BIO-INSPIRED DESIGN

5.1. Polarization. The performance of the parallel and bio designs were each simulated with a fixed mass flow rate, and with WB fixed stoichiometry, as described previously. The polarization curves obtained are given in Figure 6.

It is immediately noticeable that there is no large discrepancy in fuel cell performance between the cases presented here, as has often been observed in previous works. However, such large variations in performance are usually only seen at high current densities in the mass-transport dominated region as the result of significantly different mechanisms of mass transport, such as the introduction of under-rib flow in interdigitated style designs. In the cases considered here, mass transport from channel to catalyst layers is solely diffusive in both desgins, so no major difference in fuel cell unit performance was expected. Instead,

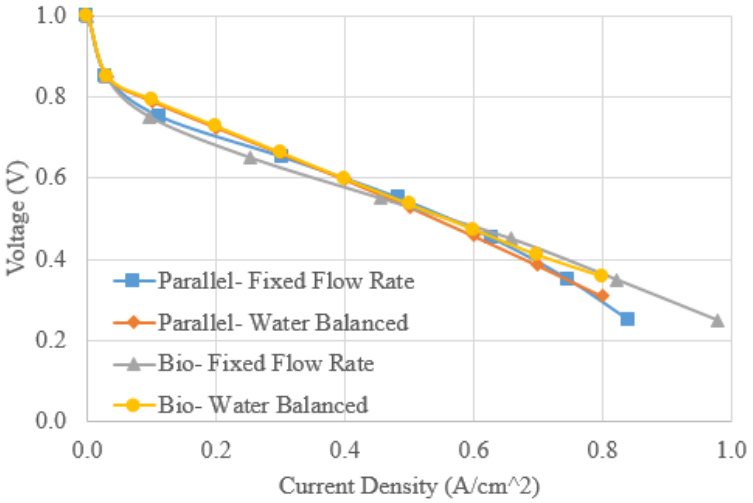

Figure 6. Polarization curves obtained from CFD results

the improvement seen in polarization performance is only incremental, while the main difference in performance of the channels is the improved distribution of reactants and removal of products over the active area, and the reduction of pressure loss across the flow field.

5.2. Power Output Per Pumping Power. In order to gage the performance of the parallel and bio designs in their ability to achieve minimal pressure losses, and therefore minimal auxiliary system requirements, the fuel cell power output per unit pumping power required was calculated for both designs. The power required to supply a fuel cell compressor, $\dot{W}_c$, at a specified mass flow rate, $\dot{m}$, and at a given inlet pressure, P_{in}, was derived for an isentropic compression process, and correct for real loss effects by the isentropic efficiency, η_c, and is given as

$$\dot{W}_c = \frac{1}{\eta_c}\dot{m}c_pT_0\left(\left(\frac{P_{in}}{P_0}\right)^{\frac{k-1}{k}} - 1\right), \tag{12}$$

where c_p is the constant pressure specific heat of the supply gas, T_0 and P_0 are the ambient temperature and pressure, and k is the ratio of specific heats. Using Equation 12 the compressor input work for both designs using the fixed mass flow rate case was calculated based on the pressure loss of each design. The power output of the cells were then

normalized by their respective compressor input work, and the resulting plots of normalized output power per compressor power input are given in Figure 7. As can be seen in, the bio design has a normalized output power of 2-3 times that of the parallel design at all operation points, and the same was true of the WB fixed stoichiometry case not shown in the figure. Since these designs have very low pressure losses, the pumping power required is quite small and the normalized output power of these designs is very large. This is a desirable characteristic for applications where minimizing the auxiliary system is a design constraint. As a point of reference, in previous work [31] the present authors have simulated the performance of the single serpentine design, which has a significantly higher pressure loss, and the maximum pumping power normalized power output was on the order of 10^1 as compared with 10^3 for the parallel design, and 10^4 for the bio.

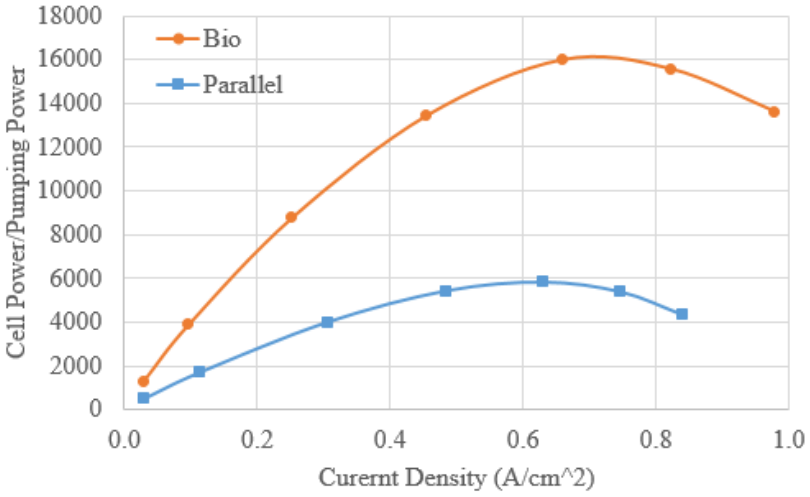

Figure 7. Fuel cell power output per pumping power input

5.3. Reactant Distribution, Product Water Removal, and Membrane Conductivity.

5.3.1. Fixed Mass Flow Rate Operation. While the bio design outperforms the parallel at high current densities in both fixed mass flow and WB fixed stoichiometry modes, the performance of all cases are nearly identical at a current density of approximately 0.5 A/cm^2. Below this point the bio design operating with fixed mass flow rate is the worst performer of all cases. The fixed mass flow rate case was the first used to compare the performance of the parallel and bio designs, and upon obtaining initial results, this phenomenon was surprising. However, investigation into the water management details of the two designs revealed that, with the fixed mass flow rate used here, the point at which the fuel cell produced enough water to fully humidify the cathode gas stream occurred between 0.5 and 0.6 A/cm^2. All operating points at lower current densities were suffering from membrane dehydration and increased ohmic losses, and all higher current densities had liquid water present at the outlet. The oxygen and water distributions at a low current density/high voltage point are shown in Figure 8. The parallel design suffered from poor distribution, and had a very large stagnation area. With the very high stoichiometries seen in the low current density range while operating with the fixed mass flow rate, sufficient oxygen was still supplied in the parallel design over most of the active area so that significant mass transport losses were not encountered, though a small area of near zero oxygen concentration is still present.The poor water removal characteristics of the parallel design actually benefited the performance in this case, as water accumulation occurred in the stagnation zone, helping to alleviate local membrane dehydration.

The bio design had significantly better reactant distribution and product removal performance, as can be seen in the contours. The oxygen distribution was significantly better than the parallel design with no areas near zero concentration, and there was less water buildup. However, in this case, product water being removed more effectively led to more severe membrane dehydration, and actually reduced performance.

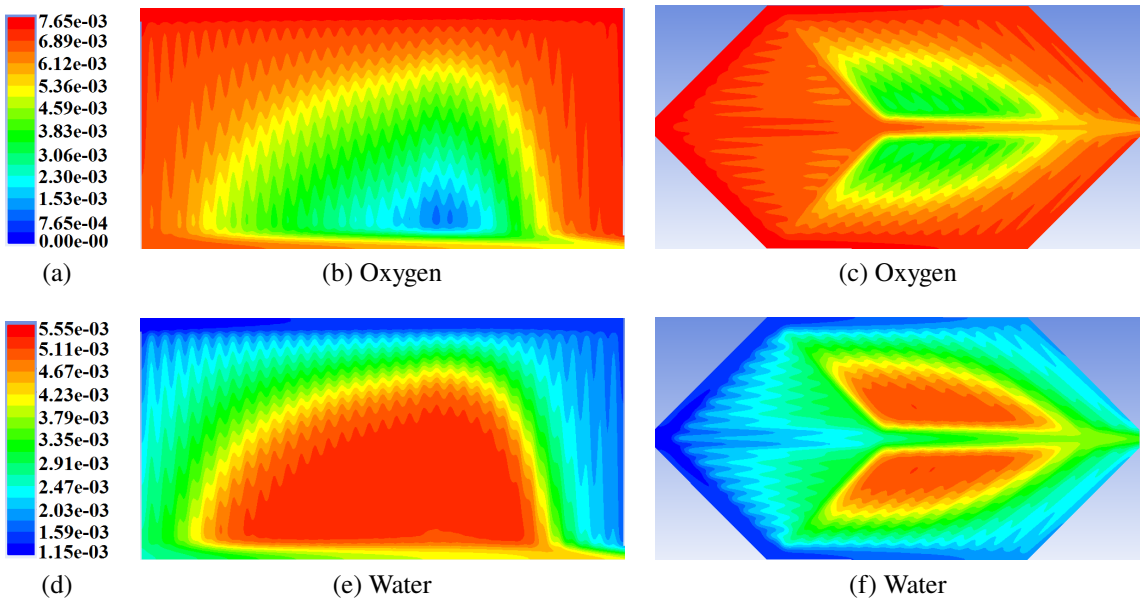

Figure 8. Fixed mass flow case: 0.65 $Volts$, catalyst-GDL interface (a) color legend for oxygen contours (b) parallel oxygen concentration (c) bio oxygen concentration (d) color legend for water contours (e) parallel water concentration (f) bio water concentration (color version available online)

5.3.2. Water Balanced Operation. It was noted that the membrane dehydration issues were alleviated once the current density, and therefore waste water production, reached a high enough point that the cathode outlet gas was fully humidified. This is what brought about the idea of calculating the proper flow rate to achieve WB operation at all current densities. The required flow rates to achieve WB operation were then calculated, and both designs were simulated again with WB fixed stoichiometry operation. The contours of oxygen and water concentration at low current density/high voltage using WB operation are given in Figure 9. Note that with the lower stoichiometry operation, the stagnation zone of the parallel design was much worse, with a large area of near zero oxygen concentration, while the bio design had a much more uniform distribution of oxygen. Furthermore, while water removal was still better in the bio design as compared to the parallel design, there was significantly more water present using WB operation, so the severe membrane dehydration issues were alleviated. This improvement in distribution not only affects the performance

directly but, as noted previously, will also serve to improve the durability and reliability of the fuel cell by reducing mechanical stresses induced by uneven water and heat distribution [4, 5].

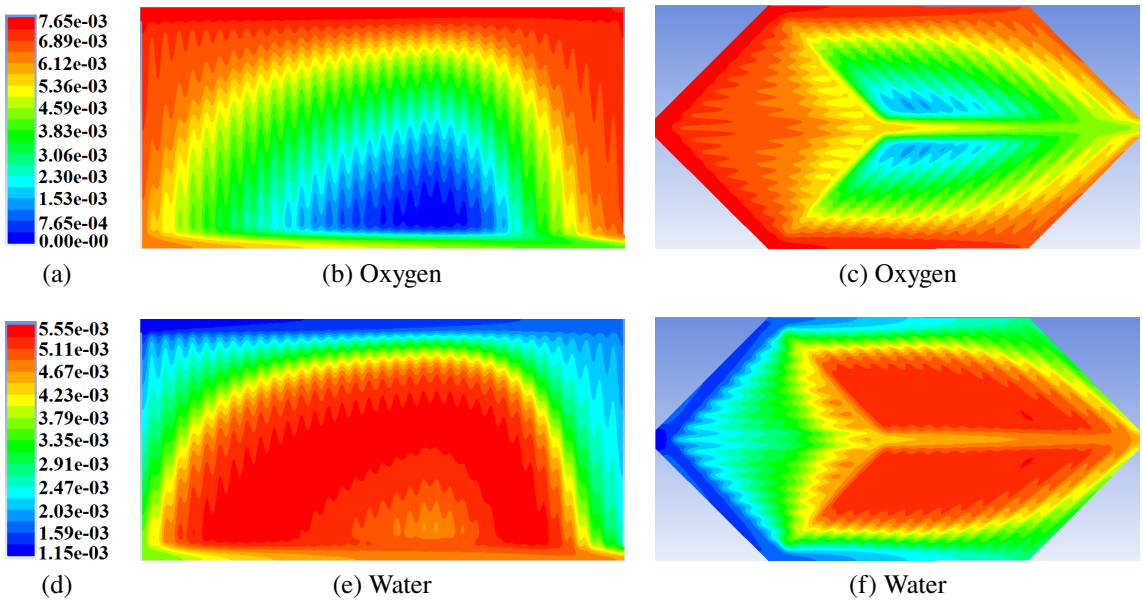

Figure 9. Water balanced case: 0.3 A/cm^2, catalyst-GDL interface. (a) color legend for oxygen contours (b) parallel oxygen concentration (c) bio oxygen concentration (d) color legend for water contours (e) parallel water concentration (f) bio water concentration (color version available online)

Using this operating scheme, the high ohmic losses incurred in protonic transport due to membrane dehydration were eliminated. The average protonic conductivity of the membrane as predicted by the Springer et al. model [32] (which is used by the computational package) for both cases is shown in Figure 10. The protonic conductivity of the membrane using WB operation was much higher at low current densities, and was relatively constant over most of the range of operation. At greater than approximately 0.6 A/cm^2 the protonic conductivity of the fixed mass flow case surpassed that of the WB case due to the presence of liquid water. Using WB operation, the polarization performance of the parallel and

bio designs were nearly identical at low current densities in the activation and ohmic loss dominated regions, and the bio design was better at high current density, due to its better distribution performance, in the mass transport limited region. Thus, using WB constant stoichiometry operation can eliminate membrane dehydration problems when using dry supply gas in designs with good water removal characteristics such as bio-designs, while still avoiding flooding issues.

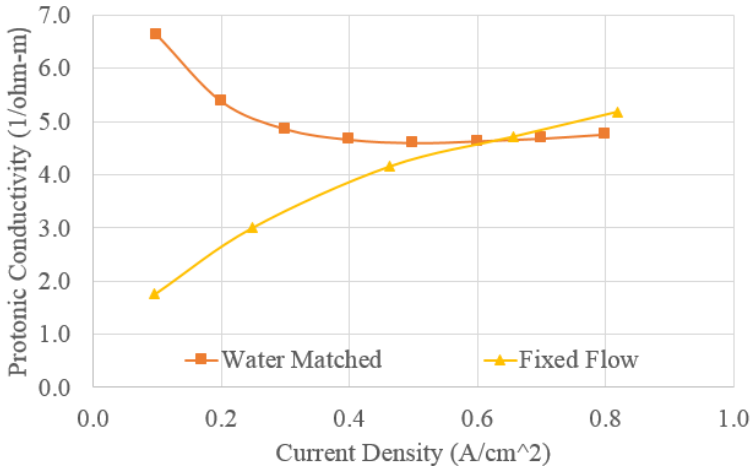

Figure 10. Average membrane water content and protonic conductivity of the bio design for both fixed flow rate and water balanced operating cases

6. SUMMARY AND CONCLUSIONS

The performance requirements of biological flow structures have been examined to identify their main geometric characteristics, and the area of applicability of bio-inspired design to fuel cell flow field design. The main driving requirement which determines the shape of biological flow structures is to achieve good distribution with minimal flow losses. Based on this performance requirement, the operating regime which has been identified for the application of bio design to fuel cell flow fields is that the dominating system requirement

is to have a minimal auxiliary system, such as a case where an extremely lightweight system is required. Using the geometric characteristics of biological flow structures, a design approach has been outlined for generating bio designs as follows:

1. Use branching geometry
2. Take advantage of symmetry when possible
3. Channel should be sized proportionally to their volume flow requirements (D^3 law)
4. Branching angles should not be extreme (avoid 90 degree bends)
5. Do not constrain the flow field geometry to the traditional rectangular area
6. Avoid preferential flow paths- match resistance with available potential
7. Avoid interdigitation

In accordance with the design goal of using a minimal auxiliary system, operating conditions were chosen which can be achieved with this goal, namely using a relatively low operating temperature with un-treated air as the cathode supply gas. In order to alleviate the water management issues of membrane dehydration at low current density, or flooding at high current density encountered when operating with un-treated atmospheric air, a new method of determining operation conditions was developed. This method matches the cathode mass flow rate to the production rate of water in the fuel cell such that the outlet relative humidity is near 100% for a given rise in temperature of the cathode supply gas. This operating mode is referred to as Water Balanced (WB) operation.

Furthermore, to demonstrate the application of these bio-inspired design principles and operating methods, a 25 cm^2 design was created, and its performance was simulated using computational modeling, along with a traditional parallel design as a reference. The purpose of the example geometry is to demonstrate that, even without optimization, through the application of these design principles, flow fields may be created with better distribution performance at lower pressure drop than the best conventional low-pressure drop design has to offer. The two designs were simulated with both fixed mass flow rates, and WB operation conditions. The bio design was shown to have a power output per pumping power input

of 2-3 times greater than that of the parallel design, as well as maintaining significantly better reactant distribution and product removal performance in all cases. Additionally, the performance of both designs were shown to improve when using WB operating conditions.

ACKNOWLEDGMENTS

This work was supported by the National Science Foundation under the grant No. CMMI-1131659.

REFERENCES

[1] R. O'Hayre, S.-W. Cha, W. Colella, F. B. Prinz, Fuel Cell Fundamentals, 2nd Edition, John Wiley & Sons, 2009.

[2] N. Muradov, Emission-free fuel reformers for mobile and portable fuel cell applications, Journal of Power Sources 118 (1-2) (2003) 320–324. doi:10.1016/S0378-7753(03)00078-8.

[3] S. E. Wright, Comparison of the theoretical performance potential of fuel cells and heat engines, Renewable Energy 29 (2) (2004) 179–195. doi:10.1016/S0960-1481(03)00191-5.

[4] J. Wang, Barriers of scaling-up fuel cells: Cost, durability and reliability, Energy 80 (2015) 509–521. doi:10.1016/j.energy.2014.12.007.
URL http://dx.doi.org/10.1016/j.energy.2014.12.007

[5] J. Wang, Theory and practice of flow field designs for fuel cell scaling-up: A critical review, Applied Energydoi:10.1016/j.apenergy.2015.01.032.
URL http://linkinghub.elsevier.com/retrieve/pii/S0306261915000380

[6] J. Wu, Q. Liu, H. Fang, Toward the optimization of operating conditions for hydrogen polymer electrolyte fuel cells, Journal of Power Sources 156 (2) (2006) 388–399. doi:10.1016/j.jpowsour.2005.05.091.

[7] A. P. Manso, F. F. Marzo, J. Barranco, X. Garikano, M. Garmendia Mujika, Influence of geometric parameters of the flow fields on the performance of a PEM fuel cell. A review, International Journal of Hydrogen Energy 37 (20) (2012) 15256–15287. doi:10.1016/j.ijhydene.2012.07.076.
URL http://dx.doi.org/10.1016/j.ijhydene.2012.07.076

[8] H.-W. Wu, A review of recent development: Transport and performance modeling of PEM fuel cells, Applied Energy 165 (2016) 81–106. doi:10.1016/j.apenergy.2015.12.075.
URL http://linkinghub.elsevier.com/retrieve/pii/S0306261915016487

[9] K. Tüber, A. Oedegaard, M. Hermann, C. Hebling, Investigation of fractal flow-fields in portable proton exchange membrane and direct methanol fuel cells, Journal of Power Sources 131 (2004) 175–181. doi:10.1016/j.jpowsour.2003.11.078.

[10] J. P. Kloess, X. Wang, J. Liu, Z. Shi, L. Guessous, Investigation of bio-inspired flow channel designs for bipolar plates in proton exchange membrane fuel cells, Journal of Power Sources 188 (1) (2009) 132–140. doi:10.1016/j.jpowsour.2008.11.123.

[11] C. T. Wang, C. P. Chang, C. K. Shaw, J. Y. Cheng, Fuel Cell Bionic Flow Slab Design, Journal of Fuel Cell Science and Technology 7 (1) (2010) 011009. doi:10.1115/1.3009281.
URL http://link.aip.org/link/JFCSAU/v7/i1/p011009/s1&Agg=doi

[12] C. T. Wang, Y. C. Hu, P. L. Zheng, Novel biometric flow slab design for improvement of PEMFC performance, Applied Energy 87 (4) (2010) 1366–1375. doi:10.1016/j.apenergy.2009.05.039.
URL http://dx.doi.org/10.1016/j.apenergy.2009.05.039

[13] J. M. Currie, Biomimetic Design Applied to the Redesign of a PEM Fuel Cell Flow Field by Biomimetic Design Applied to the Redesign of a PEM Fuel Cell, Ph.D. thesis (2010).

[14] R. Roshandel, F. Arbabi, G. K. Moghaddam, Simulation of an innovative flow-field design based on a bio inspired pattern for PEM fuel cells, Renewable Energy 41 (2012) 86–95. doi:10.1016/j.renene.2011.10.008.
URL http://dx.doi.org/10.1016/j.renene.2011.10.008

[15] N. Guo, M. C. Leu, U. O. Koylu, Bio-inspired flow field designs for polymer electrolyte membrane fuel cells, International Journal of Hydrogen Energy 39 (36) (2014) 21185–21195. doi:10.1016/j.ijhydene.2014.10.069.
URL http://linkinghub.elsevier.com/retrieve/pii/S0360319914029097

[16] B. P. Saripella, U. O. Koylu, M. C. Leu, Experimental and Computational Evaluation of Performance and Water Management Characteristics of a Bio-Inspired Proton Exchange Membrane Fuel Cell, Journal of Fuel Cell Science and Technology 12 (6) (2015) 061007. doi:10.1115/1.4032041.

[17] A. Arvay, J. French, J. Wang, X. Peng, A. M. Kannan, Modeling and Simulation of Biologically Inspired Flow Field Designs for Proton Exchange Membrane Fuel Cells, The Open Electrochemistry Journal (2015) 1–9.

[18] A. Ozden, M. Ercelik, D. Ouellette, C. O. Colpan, H. Ganjehsarabi, F. Hamdullahpur, Designing, modeling and performance investigation of bio-inspired flow field based DMFCs, International Journal of Hydrogen Energy (2017) 1–13doi:10.1016/j.ijhydene.2017.01.007.
URL http://dx.doi.org/10.1016/j.ijhydene.2017.01.007

[19] T. F. Sherman, On connecting large vessels to small. The meaning of Murray's law., The Journal of general physiology 78 (4) (1981) 431–453. doi:10.1085/jgp.78.4.431.

[20] C. D. Murray, The Physiological Principle of Minimum Work I. The Vascular System and the Cost of Blood Volume, Proceedings of the National Academy of Science 12 (3) (1926) 207–214.

[21] C. D. Murray, The Physiological Principal Of Minimum Work Applied To The Angle Of Branching Of Arteries, Journal of General Physiology 9 (1926) 835–841. arXiv:0103065v2, doi:10.1103/PhysRevC.71.064610.

[22] T. V. Nguyen, A Gas Distributor Design for Proton-Exchange-Membrane Fuel Cells, Journal of The Electrochemical Society 143 (5) (1996) L103. doi:10.1149/1.1836666.

[23] J. P. Feser, a. K. Prasad, S. G. Advani, On the relative influence of convection in serpentine flow fields of PEM fuel cells, Journal of Power Sources 161 (1) (2006) 404–412. doi:10.1016/j.jpowsour.2006.04.129.

[24] D. C. Wilcox, Basic Fluid Mechanics, 5th Edition, 2012.

[25] Z. Qi, A. Kaufman, PEM fuel cell stacks operated under dry-reactant conditions, Journal of Power Sources 109 (2) (2002) 469–476. doi:10.1016/S0378-7753(02)00111-8.

[26] M. V. Williams, H. R. Kunz, J. M. Fenton, Operation of Nafion(R)-based PEM fuel cells with no external humidification: Influence of operating conditions and gas diffusion layers, Journal of Power Sources 135 (1-2) (2004) 122–134. doi:10.1016/j.jpowsour.2004.04.010.

[27] X. Li, I. Sabir, J. Park, A flow channel design procedure for PEM fuel cells with effective water removal, Journal of Power Sources 163 (2) (2007) 933–942. doi:10.1016/j.jpowsour.2006.10.015.

[28] A. Iranzo, M. Muñoz, F. Rosa, J. Pino, Numerical model for the performance prediction of a PEM fuel cell. Model results and experimental validation, International Journal of Hydrogen Energy 35 (20) (2010) 11533–11550. doi:10.1016/j.ijhydene.2010.04.129.

[29] Ansys academic research, release 15.0, help system, fuel cell modules manuel.

[30] A. Arvay, A. Ahmed, X. Peng, A. M. Kannan, Convergence criteria establishment for 3D simulation of proton exchange membrane fuel cell, International Journal of Hydrogen Energy 37 (3) (2011) 2482–2489. doi:10.1016/j.ijhydene.2011.11.005.
URL http://dx.doi.org/10.1016/j.ijhydene.2011.11.005

[31] J. D. Heck, Bio-inspired flow fields for pem fuel cells- decoupling pressure and distribution effects on performance and identifying design opportunities, Masters Thesis, Missouri University of Science and Technology,2017.

[32] T. E. Springer, T. A. Zawodzinski, S. Gottesfeld, Polymer Electrolyte Fuel Cell Model, J. Electrochem. Soc. 138 (8) (1991) 2331–2342.

SECTION

2. CONCLUSIONS

It has been shown that the effect on system performance, caused by the different pressure loss characteristics of flow fields, can indeed be significant in PEMFCs. A method of decoupling the performance effects of pressure and reactant distribution has been demonstrated which normalizes the effects of pressure between different flow field designs, and thereby provides fuel cell designers a tool whereby the relative merits of different flow field designs can be better compared. This method was demonstrated by application to the traditional parallel and serpentine flow fields. It was shown that, under the operating conditions used, the fuel cell utilizing the serpentine flow field outperformed that using the parallel flow field by 17% at the peak power density point. However, of the 17% improvement, 12% was due to improved reactant distribution of the serpentine design, while the remaining 5% enhancement was from effects of the serpentine design's higher pressure loss. It was furthermore demonstrated from previous literature that, in some flow field designs, the effects from increased pressure loss are the primary contributor to fuel cell unit performance enhancement. This is an undesirable characteristic for a new flow field, as the same effect can be achieved by simply operating an existing design at a slightly higher back pressure.

The opportunity for application of bio design to fuel cell flow fields was also investigated. The performance requirements for biological flow structures were examined, and it was determined that the most important outcome for a biological flow system is to achieve properly proportioned flow distribution with minimal pressure losses. Since the requirement to achieve proper flow distribution exists for all fuel cell flow fields, the area

of particular applicability for bio design must be when minimal pressure loss is a dominate design constraint, such as when a minimal auxiliary system is desired. In keeping with this design goal, a set of design principles was developed for creating bio designs as follows:

1. Use branching geometry
2. Take advantage of symmetry when possible
3. Channel should be sized proportionally to their volume flow requirements (D^3 law)
4. Branching angles should not be extreme (avoid 90 degree bends)
5. Do not constrain the flow field geometry to the traditional rectangular area
6. Avoid preferential flow paths- Match resistance with available potential
7. Avoid interdigitation

The application of these design principles was demonstrated by creating an example bio design. The performance of the bio design was then simulated, along with the traditional parallel design as a reference. Operating conditions for testing these designs were chosen in keeping with the goal of minimizing the auxiliary system, so a relatively low operating temperature and ambient back pressure were used with un-treated atmospheric air supplied for the cathode gas. When operating with low humidity supply gas, it was observed that performance was limited by membraned dehydration at low current densities when operating under fixed mass flow rate conditions, while liquid water accumulation would still occur at high current density. In order to alleviate these water management issues, a new method of determining operating conditions was developed which has been termed Water Balanced (WB) operation. Using WB operation, the supply rate of low humidity air at the cathode inlet is matched to the production rate of waste water from the electrochemical reactions such that the cathode gas is fully humidified at the outlet temperature. The bio and parallel designs were both run with fixed mass flow rates and WB operation. In order to demonstrate the reduced pressure losses in the bio design, the fuel cell power output per pumping power required was calculated for both designs, and it was shown that the bio design performed 2-3 times better than the parallel design for both cases, while also maintaining better reactant

distribution. Furthermore, it was shown that both the bio and parallel designs performed better with WB operating conditions, which successfully eliminated membrane dehydration issues.

VITA

Joshua David Heck was born December 11th, 1990, in Overland Park, Kansas, and grew up in the Kansas City, Missouri area. He received his B.S. in Mechanical Engineering from the Missouri University of Science and Technology in May, 2015.

During the course of his graduate study, he authored two papers for publication, which are contained in this thesis. In May, 2017 he received his MS in Mechanical Engineering under the advisement of Dr. Umit O. Koylu, and Dr. Ming C. Leu.